# Time-dependent Scrape-Off Layer simulations with JOREK for detachment control

Maris, Daniël

*Award date:*
2024

Department of Applied Physics and Science Education

# Time-dependent Scrape-Off Layer simulations with JOREK for detachment control

by

**D. Maris**

MSC THESIS

**Assessment committee**

| | |
|---|---|
| Member 1 (chair): | Prof.dr. R.J.E. Jaspers |
| Member 2: | Dr. H.J. de Blank |
| Member 3: | Dr. P. Nguygen |
| Advisory member 1: | Dr. T. Ravensbergen |
| Advisory member 2: | Dr. J. Artola |

**Graduation**

| | |
|---|---|
| Program: | Science and Technology of Nuclear Fusion |
| Capacity group: | Science and Technology of Nuclear Fusion |
| Supervisor: | Prof.dr. R.J.E. Jaspers |
| Date of defense: | June 26, 2024 |
| Student ID: | 1367803 |
| Study load (ECTS): | 45 ECTS |

The research of this thesis has been carried out in collaboration with *ITER Organization*.
This thesis is public and Open Access.

This thesis has been realized in accordance with the regulations as stated in the TU/e Code of Scientific Conduct.

**Abstract**

Climate change calls for energy transition towards sustainable sources such as nuclear fusion. Nuclear fusion aims to fuse light isotopes into heavier ones, releasing heat which can be converted into electricity. Major future fusion experiment ITER will magnetically confine a hot plasma in a torus. The power generated in the hot confined core ends end up in a narrow regions outside the core called the scrape-off layer (SOL), which ends on either side on a wall target. One of the open issues in fusion is how to keep the power on these targets below material limits. This is known as the exhaust problem, which major future experiment ITER plans to solve by keeping the SOL in the semi-detached regime. In this regime, volumetric energy, momentum and particle losses reduce the fluxes to the targets while maintaining high core performance. This regime requires active feedback control to avoid excessive heat loads or radiative collapse. To aid such controller design, high fidelity dynamic SOL simulations are desirable, as they can be used to understand the system better and thus also extract control quantities such as timescales, transfer functions and relation of measured signals to the whole SOL state. This work improved the kinetic neutral model of MHD code JOREK, which is inherently dynamic, as it was found to be lacking in benchmarks against the widely accepted equilibrium code SOLPS. JOREK's kinetic neutral model's numerical particle confinement was improved from errors of $\sim$100% to $\sim$3% of the puff rate. Furthermore, better far SOL heat flux boundary condition and perpendicular heat flux assumption were implemented, and pumping capability was added. Nevertheless, the improved version was still lacking in benchmarks against SOLPS, which is likely mainly caused by the missing neutral-neutral collisions and molecules in JOREK's neutral physics model.

After these improvements, JOREK's kinetic neutral model was used to produce proof of concept preliminary control results, so that once JOREK is improved, this can be repeated with higher fidelity. The investigation focused on the SOL dynamics in the control loop with gas puff as actuator and divertor shunt as diagnostic. As the divertor shunt indirectly measures the SOL current, a post-processing routine was written to determine the SOL current from the SOL state. It was found that both the peak heat flux and the post-processed SOL current had response times of $\sim$5ms which is extremely small compared to the $\sim$0.5s response time of the gas puff due to the long pipes, and upper estimate of $\sim$0.1s of the SOL self induction timescale. This result was expected from current devices and previous SOL timescale estimates. It means that in a control loop, the SOL can be approximated well as a static (nonlinear) gain without internal dynamics, which is beneficial for the control model's simplicity. It also means that the ability of the control loop to keep the system within operational limits depends on the timescale and extent of perturbations on the SOL state due to changes imposed in the interaction with the core, such as $dP_{SOL}$, $dn_{e,u}$ and L-H transitions. This requires further research for which JOREK is well suited. Furthermore, the peak heat flux and SOL current are observed to be correlated, albeit not one-to-one, when self induction is ignored. Further investigation is required to determine whether the relation is close to one-to-one for slow, small amplitude changes around a semi-detached state when self-induction is included.

# Contents

# Chapter 1:
# Introduction

One of the largest challenges facing humanity today is climate change, and part of the solution is in the transition away from fossil fuels to sustainable energy. While wind and solar power have intrinsic low power density and a mismatch between supply and demand without clear large scale storage solutions, and nuclear fission is feared for its radioactive waste products, nuclear fusion is expected to be capable of producing electricity on demand at high power density without long-lived nuclear waste.

To prove the concept of power generation through nuclear fusion, the experimental facility ITER is being constructed, in which a magnetically confined plasma is planned to output more power than is necessary to heat the plasma in a device called a tokamak.

The magnetic configuration of high performance fusion devices generates a large power flow along the so called scrape-off layer (SOL) to the wall targets in a region called the divertor, which left unmitigated would ruin the mechanical properties of the most resilient materials on earth. This problem is known as the exhaust problem, and it necessitates volumetric energy and particle losses in the SOL [1]. These losses can be induced by seeding impurities, which radiate and thus lower the power to the targets, and by increasing fuelling which leads to recycling. Recycling lowers the divertor temperature, causing recombination and thus radiating neutrals and lowered particle fluxes to the target. This SOL state is called detachment. However, losing too much power can lead to a so called radiative collapse [2] which can trigger a disruption, i.e. a magnetohydrodynamic (MHD) instability which can severely damage a high performance device such as ITER [3], and must therefore be avoided at all cost. Thus the detachment state must be well understood so that it can be carefully controlled in power generating devices.

Since detachment controllers have to respond to and compensate changes in the SOL state, it is vital that not just steady states but also the dynamics of the SOL are understood. As current day fusion devices are different from power generating devices, an important method to obtain information on future devices is by means of modelling using simulation codes. Therefore it is desirable to have a reliable SOL simulation code available to study such devices in advance to design a detachment state controller.

Although development of high fidelity dynamic SOL simulation codes is still in its infancy, recently a leap forward was taken when the MHD code JOREK gained kinetic neutral capability [4]. As this kinetic neutral model has not been extensively benchmarked yet and it misses important physics, there is strong motive to develop this code further, so that it can be used in the future to aid controller design.

To gain confidence in the robustness of the detachment control system for ITER, it is vital to test these systems for low performance plasmas in the Pre-Fusion Power Operation (PFPO) experimental phase [5] (which is now renamed Start of Research Operation, SRO). To make the most of the ITER experimental campaign within the time limits of the nuclear license, the budget, and the goal of achieving fusion power, the experimental schedule is tight, thus there is the need to design the required control systems for these low performance plasmas in advance as well [6]. To design the detachment controller, knowledge is needed on the actuator, on the diagnostic used and on the SOL system itself.

The actuator is the combination of set of valves controlling the (impurity) gas puffing rate and their $\sim$20m long pipes leading the gas into the vessel, and it has been studied in [7].

For the diagnostic, there are multiple options [8], such as optical methods [9], bolometry [10, 11], Langmuir probes [12] and the divertor shunt [13]. Due to its simplicity and lack of lifetime issues from neutron irradiation and plasma proximity, it would be ideal to be able to use the divertor shunts as diagnostic. Previously, the potential of the divertor shunts to fulfill this role for detachment control in ITER has been verified by deriving relations of (1) peak heat flux to SOL target current and (2)

SOL target current to divertor shunt voltages from simulations, which were such that a measured divertor shunt voltage can be translated into a corresponding peak heat flux [14], which is the relevant quantity as the divertor targets will be designed to withstand a certain maximum steady state power flux [15], above which recrystallization will occur. Thus the divertor shunts can in principle be used as diagnostic. However, relation (1) was determined from static SOLPS [16] simulations, meaning that reality, which is dynamic, is likely different.

Although actuator and diagnostic have been studied, no systematic investigation into the ITER SOL dynamics for the purpose of detachment control has been done before. Therefore this project aims to study the SOL system in the control loop given in figure 1.1 to answer the question: *What are the basics of SOL dynamics relevant to ITER detachment control with divertor shunts as diagnostic?* With basics being the ingredients necessary to build a controller; i.e. the system timescales, transfer function, usability of SOL current as diagnostic and compatibility of SOL dynamics with actuator and diagnostic for control purposes.

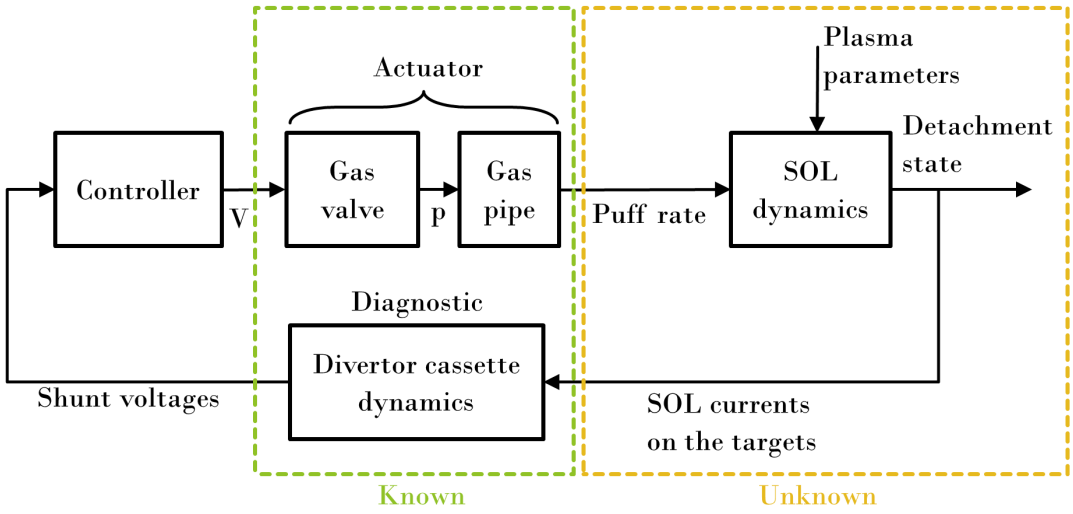


*Figure 1.1: Schematic of the ITER detachment control loop using divertor shunts as diagnostic with the focus of the current work on the SOL dynamics. Both actuator [7] and divertor cassette dynamics [14] have been investigated before, so before the control system can be designed, first the SOL dynamics producing the detachment state from the puff rate and plasma parameters must be investigated.*

This research will be carried out as an internship at ITER, in close collaboration with experts on JOREK and on ITER control, and with access to the Scientific Data and Computing Center (SDCC), i.e. ITER's high-performance computing system.

To answer the research question, this work will; (I) *determine the evolution of the relation between peak heat flux and target current*, to see whether and how peak heat flux can be determined from target current in dynamic situations; (II) *determine SOL system timescales*, since these timescales are useful for the control engineer in understanding the plant, and necessary to establish whether the response time, given by the time it takes to observe and act on an unwanted change in the detachment state, is low enough to control the system; (III) *determine a transfer function which describes the relation between puff rate and target current*, using sinusoidal puffing input to generate a frequency response function (FRF) from which a transfer function can be found to simplify the complex kinetic neutral - MHD system into an understandable input-response system for designing a controller; (IV) *determine whether the dynamic detachment state can be controlled using divertor shunt measurements as diagnostic*, or in other words, whether the relation at (I), the shunt voltage sensitivity, the timescales (II), and the input output relation of the plant (III) are all compatible such that this control loop could in principle be closed by a controller. To answer the subquestions requires an adaptation of the JOREK

kinetic neutral model code, namely a way to determine the SOL current from JOREK simulations, as that is the output of the plant in the control loop.

The necessary background theory and previous results will be discussed next (chapter 2), after which the improvements and benchmark of JOREK's kinetic neutral model will be shown (chapter 3), followed by the preparations to execute the dynamic SOL studies (chapter 4), culminating in initial answers to the control questions (5), after which the whole project will be discussed and concluded (chapter 6).

# Chapter 2:
# State-of-the-art

This chapter contains the general background theory necessary to understand the rest of report. First an introduction to the scrape-off layer will be given, after which the previous results on the atuator and diagnostic will be discussed, followed by an introduction to simulation code JOREK and its kinetic neutral model.

## 2.1 Background scrape-off layer theory

The scrape-off layer (SOL) is the region in a plasma just outside the core of the plasma. First a basic understanding of the SOL based on [17] will be presented, after which the currents in the SOL will be discussed.

In the core of a tokamak plasma, magnetic field lines organise in layers of nested flux surfaces which never intersect the device wall. Thus plasma particles, which follow the fieldlines, are confined to the surface they are on. In the SOL, the fieldlines intersect the divertor targets. The width of the SOL is set by the local plasma transport and the applied magnetic fields and is not yet well understood. For larger devices, the SOL is predicted to be quite narrow [18]. As electrons are more mobile than ions due to their lower mass, electrons will reach the wall at higher rate until a sheath potential builds up between the wall and the plasma, restoring ambipolar transport. Since the sheath potential must stop most of the electrons and only let the tail of the velocity distribution pass, the sheath potential that builds up is a few times the electron temperature (in eV).

Depending on the conditions, the SOL can be in a variety of regimes. In the low recycling, or sheath limited, regime, the transport is dominated by this boundary sheath. The convection, driven by the plasma loss at the wall, means the electrons and ions flow to the wall, where they neutralize. This means the upstream temperature, i.e. the temperature at the intersection of the outer midplane and the separatrix, is the same as the downstream temperature, i.e. the plasma temperature at the divertor target.

At higher upstream densities, the ions hitting the wall saturate the wall and thus new ions neutralize at the wall but then re-enter the plasma. Since the plasma is hot, these neutrals will ionize again and thus flow to the wall again. This recycling can happen many times, meaning the ion flux is larger than in the low-recycling regime, thus a large downstream density is generated, as is schematically shown in figure 2.1. This new source of ions in the SOL stops the convective flow of the plasma to the target, or in other words, momentum is lost through friction. This broadens the profiles at the targets, and it means that conduction becomes the important heat transport mechanism in the plasma near the targets. Although this lowers the peak heat flux by broadening the profiles at the target, the total power to the targets is unchanged. Furthermore, the density dilution with the ionised neutrals causes the ion temperature at the target to be much lower than the upstream ion temperature. This regime is called the high recycling or conduction limited regime. In both low and high recycling regime, the static pressure at the target is approximately half the upstream static pressure, as there are no volumetric energy losses.

If there are volumetric energy losses in the SOL, from electron decay from cold neutrals or radiation from injected impurities, then the temperature in the SOL can be low enough that ions recombine in the SOL (bulk recombination), and thus both energy and particle fluxes to the target can vanish. This is called detachment, as the energy and particle fluxes from the core end up in the gas, from which it spreads out over the whole wall, rather than just ending up on the divertor target. See figure 2.1 for a schematic explanation of detachment. This makes it possible to have low total heat flux on the target,

which is required to protect the divertor, even with high heat flux through the separatrix, which is necessary for high performance. Note that low plasma heat flux on the target with high particle heat flux, such as in a high recycling seeded scenario, still generates a large target heat flux, due to the 13.6eV energy deposited on the wall when a plasma ion recombines at the target. For ITER, therefore, both volumetric particle and energy loss are required, thus ITER must be in the detached state [19].

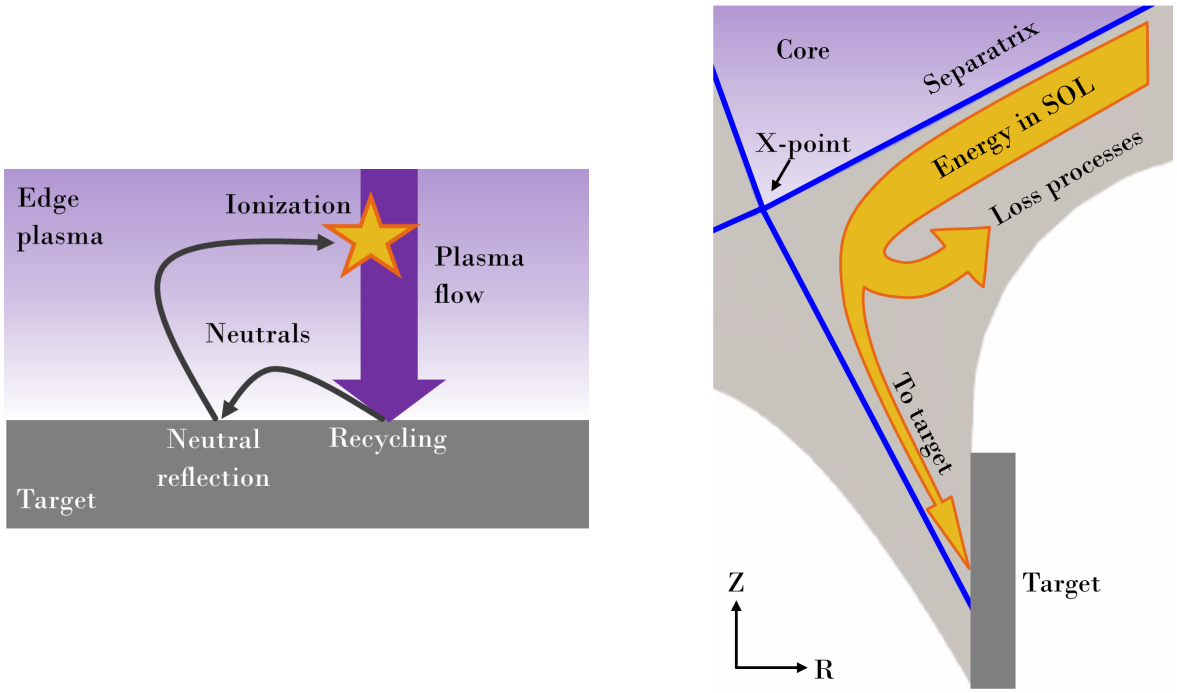


*Figure 2.1: Left: Concept of recycling leading to build-up of density. A single atom passes multiple times to the target, hence the name recycling. The increase in density lowers the target temperature thus allowing for low temperature loss mechanisms such as radiation and bulk recombination to become large sinks, thus effectively cushioning the incoming heat- and particle fluxes. Right: The detached state in the SOL of a tokamak. Most of the energy flowing into the SOL from the separatrix does not hit the target but instead is lost in the SOL through radiation and recombination. This is a fine balance where too little detachment can cause damaging heatfluxes to the target, but too much detachment can trigger a radiative collapse which can lead to a disruption, a large scale plasma instability which can damage the whole device.*

### 2.1.1 SOL current origin

Due to the torus geometry of tokamaks like ITER, there is more area on the outboard side than on the inboard side. Together with geometry dependent drifts and turbulent transport, this means that the plasma power to the outboard side is usually larger than to the inboard side by a factor 2.5 [20]. Therefore the inner target often detaches earlier than the outer target [21], and the temperature at the inboard side is usually smaller than on the outboard side. The sheath potential is therefore different for the inboard and outboard side, meaning there is an electric potential difference which can drive a current between the outboard and inboard side, as schematically shown in figure 2.2. Indeed this thermoelectric current is observed [22] and in normal configuration comes out of the outer target, runs through the SOL into the inner target, and then back through the divertor cassette to the outer target again (see figure 2.2). In reality it is not a single current line but rather a current density profile on the targets, with some current flowing in the private flux region (PFR) between the X-point and the dome.

Furthermore, the SOL current can also be driven by a pressure rather than temperature gradient, and it is limited by the saturation current density, which is the maximum current density which can be drawn to the target due to the finite amount of ions available.

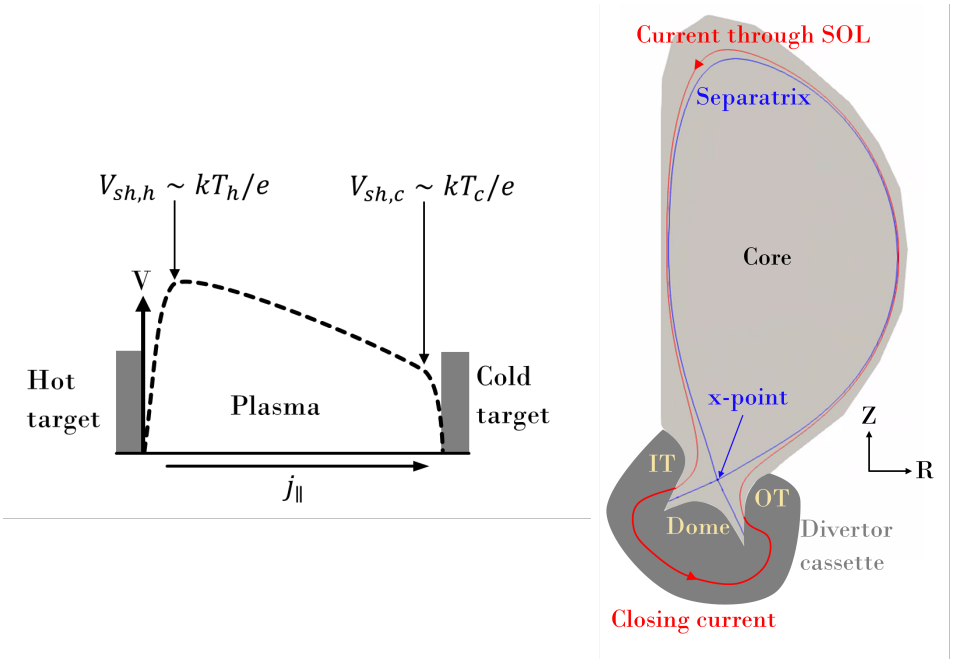


*Figure 2.2: Schematic of the SOL current origin (left) and direction in a poloidal cross section of ITER's geometry (right). SOL current develops due to a difference in target temperature and pressure between the inner and outer target. This can be understood by the different resulting sheath potential at the two target, leading to a voltage drop over the SOL thus driving a current. Since the hot target is usually the outer target, the SOL current flows out of the outer target (OT), through the SOL (just outside the separatrix) into the inner target (IT), through the divertor cassette and closing the loop back to the outer target. Since the divertor shunts directly measure voltage differences in the divertor cassette, this integrated target current can be measured with the divertor shunts as verified in [14].*

## 2.2 Previous results on the actuator: the gas puff

The detachment state can be changed by introducing particles into the divertor from outside of the plasma, which can either be impurities or fuel, and they can either be puffed or injected as pellets [23]. Fuel particles increase the plasma density and thus the recycling and neutral radiation, while impurity species can radiate significantly in an ionised state. The pumping rate is not ideal as an actuator because the rate depends on the neutral pressure and temperature in the divertor, and there will be limited pumps available which need to regenerate as well, while the pump valves are slow to open and close [24]. As pellets will be used for core density control, puffing is foreseen as the main actuator for divertor control.

Due to the nuclear nature of ITER, the gas valves and gas supply must be outside the bioshield, meaning puffing pipes are ∼20m making the response time slow. An experimental study into the achievable response time using these pipes found a lower limit of ∼0.5s for mixtures of impurity and carrier gas, as the pressure inside the valve is the main driver of response time [7]. This timescale will be taken as a lower limit for the current study, as even though in PFPO-1 scenario's there will be no impurity injection, the main component of the fastest response time gas mixtures was carrier gas, meaning that the response time in PFPO-1 will be similar.

One of the actuator's potential concerns is failure of a gas valve to (stay) open [23]. Depending on what gas should be puffed from the pipe this could lead to a loss of seeding or to a lowering of the total hydrogen puff rate, both of which could cause the plasma to rapidly re-attach. To avoid re-attachment, the other gas pipes should compensate for the failure. An open control question is on what timescale this re-attachment occurs.

## 2.3 Previous results on the diagnostic: the divertor shunt

The divertor shunts are voltage pairs embedded in the divertor cassette body as can be seen in figure 2.3. As they are fully hidden behind the divertor itself, they are not exposed to high heatfluxes unlike for example Langmuir probes, which are not expected to make it into the fusion power operation (FPO) phase (now called the DT phase for deuterium tritium, the fusion fuels). Furthermore, since voltage lines are simple conductors, they do not degrade heavily due to neutron irradiation, unlike for example the mirrors necessary for spectroscopic methods. Thus, as mentioned in the introduction, it would be ideal to be able to use the divertor shunts measurements as a diagnostic of the detachment state due to its simplicity and it being far away from the plasma compared to other possible diagnostics.

In [14], it was found that the frequency response of the divertor shunt measurements to SOL currents has a sensitivity of 0.1kA. The gain starts decreasing by a decade for each frequency decade after 1Hz, and the phase lag starts becoming noticeable for frequencies above 10Hz. Furthermore, the relation between total current and peak heat flux ($q_{peak}$) was determined for different scenario's ranging from PFPO-1 to FPO with different Ne impurity contents, see figure 2.3. It was found that for $q_{peak} > 1\text{MW/m}^2$, the sensitivity limit of 0.1kA of the divertor shunts was met, and that the relations were of such a nature that the SOL current was a reasonable indication of $q_{peak}$. As stated in the introduction, these relations were determined from static SOLPS simulations, whereas this work aims to re-investigate this relation from dynamic simulations.

## 2.4 SOL application of MHD code JOREK

In this section, the simulation code used in this work, JOREK, will be described, starting with the parts of JOREK's MHD model relevant to this work, followed by the kinetic neutral model, and ended with a comparison of kinetic neutral JOREK to SOLPS, a more widely used static SOL code.

### 2.4.1 MHD model in JOREK

JOREK [25] is a magnetohydrodynamic (MHD) code designed to model magnetically confined fusion plasmas, with a key role in the modelling of large scale plasma instabilities. MHD is the physics describing a conducting fluid in a magnetic environment such as a plasma, or in other words, Maxwell's equations applied to a conducting fluid. In the settings of the code used in this work, the MHD model is reduced, meaning the highest frequency phenomenon, the fast magnetosonic waves, are eliminated such that good accuracy can be achieved at large time steps, thus reducing simulation time. For JOREK, this reduction is done through the Ansatz method, which limits the form of the magnetic potential and in that way removes magnetosonic waves.

JOREK uses 3rd order polynomial finite elements in the poloidal plane, combined with Fourier series to represent toroidal dependencies. The finite elements are based on bicubic Bezier surfaces, which satisfy $G^1$ continuity, i.e. they are fully differentiable. This means that the poloidal plane is subdivided into small (finite) elements, on which functions, e.g. the electron density $n_e(R, Z)$, are represented by the coefficients of known polynomials, the Bezier basis functions, with 4 coefficients per basis function and 4 basis functions per element. All finite elements together then describe a continuous and fully differential surface. The finite elements are isoparametric quadrilaterals, i.e. 4 curved lines connected by 4 points, such that the grid can be a flux aligned grid, which is beneficial to

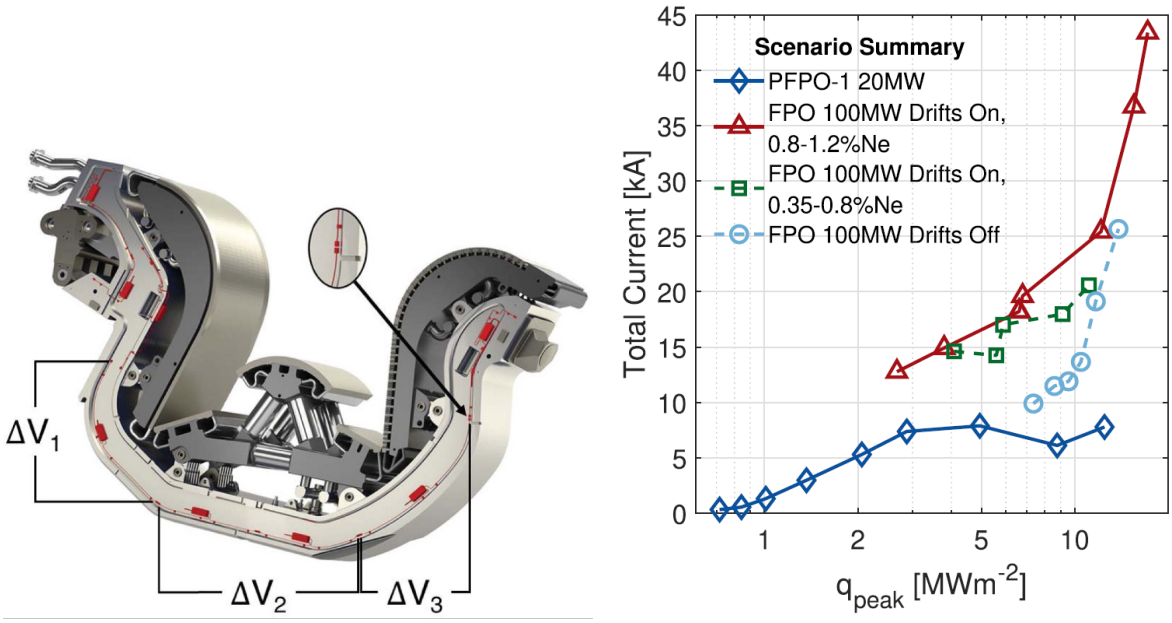


*Figure 2.3: Shunt diagnostic as diagnostic for detachment control. Left: rendering of ITER divertor cassette with shunt diagnostic. Shunt cables, i.e. conducting cables over which the voltage difference is measured, are shown in red. The measured voltages relate to the SOL current. Right: relation between SOL current and peak heat flux for different fuelling scenario's, as determined from static SOLPS simulations. Since the input parameters are known for a given shot, and the relation between SOL current and peak heat flux is mostly one-to-one, a control system could deduce the peak heat flux from the total SOL current. This means the SOL current can be used as diagnostic. This work aims to investigate this relation for a dynamic situation. Reproduced with permission from [14].*

the numerical issues generated by the large difference between parallel and perpendicular transport. The grid extends to the physical wall.

Although more advanced options are possible, this work is 2D (i.e. toroidal symmetry is assumed), and it makes use of reduced MHD with as variables the poloidal magnetic flux $\Psi$, velocity stream function $u$, toroidal current density $j$, toroidal vorticity $\omega$, mass density $\rho$, single temperature $T = T_e + T_i$, i.e. the sum of electron and ion temperatures, and parallel velocity $v_\parallel$. There are sheath boundary conditions at the walls, and the initial condition is determined from a Grad-Shafranov equilibrium solver which takes initial density, temperature, poloidal current stream function and flux profiles as input. JOREK solves the weak form of the nonlinear reduced MHD equation on the finite elements using matrix equations, and the time stepping is implicit, meaning the change in finite element coefficients is calculated from a matrix equation using a scheme which is inherently stable.

### 2.4.2 Kinetic neutral model in JOREK

Recently [4], a kinetic neutral model was developed and tested for JOREK, which means it has now become possible to do time-dependent detachment simulations with JOREK. As mentioned in section 2.1, neutrals play a key role in detachment, and it turns out that a neutral fluid model does not capture the essential dynamics well enough, thus a kinetic approach is needed. This is done by generating, tracking and destroying super-particles, which represent a certain number of neutral particles depending on their variable weight. The trajectories of these super-particles are evolved over time in real space through multiple kinetic time steps every (MHD) fluid time step. Since reactions involving the neutrals and the plasma, such as ionization, show up as sources or sinks in the MHD balance equations which are defined on the finite element grid, the real space kinetic particles are projected back every fluid time step onto the finite element grid. At every fluid time step, super particle weights are lowered

according to the local ionization rate, until the weight is below a threshold, then the whole super particle either ionises or not depending on a comparison between a generated random number and the ionisation probability. Simultaneously, new super-particles are initiated at the fluid time step in each element to reflect recombination, and at the boundary to reflect plasma sputtering and recycling. Furthermore, there is the option to puff neutral particles into the plasma. The location of this puffing can be chosen, but for this work usually was at the top of the vessel, which is one of the options in ITER.

The plasma-neutral reactions which are included in the current version of the kinetic neutral code are ionization, recombination and charge exchange. The plasma is assumed to be transparent to radiation calculated from recombination and line radiation. The kinetic neutrals are radicals, or in other words, there are no molecular interactions. Furthermore there are no neutral-neutral interactions, meaning that there's no realistic plasma pressure. Neutrals contribute to sputtering, and are reflected and absorbed at the boundary. Furthermore, there's an energy loss term representing excitation of atoms which then lose that energy through line radiation.

### 2.4.3 Difference to widely used SOL code SOLPS

SOLPS (scrape-off layer plasma simulator) is an equilibrium code coupling kinetic neutral particles (EIRENE) to a fluid code (B2). SOLPS is widely used, well benchmarked, and has for instance been the standard code to determine the design requirements for the ITER divertor [15]. Compared to SOLPS, JOREK has a simplistic physics model for the kinetic neutrals at this point. Amongst others, SOLPS tracks $T_e$ and $T_i$ individually (which is possible in JOREK, but not yet in combination with the kinetic neutrals), it has neutral-neutral interactions, molecular interactions and decay, radiation opacity, and a multiple fluid model making for example the creation of helium due to fusion reactions possible. For comprehensive comparison of JOREK to SOLPS, see table 2.1.

Both the core JOREK code [25] and SOLPS as a whole [26] have been benchmarked extensively and can thus be considered to be trustworthy in their basic functionality. However, since the kinetic neutral model of JOREK is a recent addition, it has not been benchmarked yet beyond that presented in [4], where the total power and the peak heat flux were compared against SOLPS simulations as a function of the upstream densities of both sets of simulations. Although the total power corresponded reasonably well for upstream densities up to $n_{e,u} = 2 \cdot 10^{19}\mathrm{m}^{-3}$, the peak heat flux had discrepancies up to a factor 3 even for low densities, indicating a more peaked profile for JOREK than for SOLPS.

This benchmark was done with the full SOLPS physics model rather than the selection of physics

*Table 2.1: Comparison between SOL codes JOREK (with kinetic neutrals) and SOLPS. Both models include recycling, ionisation, recombination, charge exchange and puffing interactions. Although JOREK's kinetic neutral model is not as mature as SOLPS, its advantages are in its time dependence, fuller plasma description (thus naturally including* $\mathbf{E} \times \mathbf{B}$ *drift) and shorter required simulation time. For control, time dependence is key, and thus JOREK's kinetic neutral model will be used for this project.*

| | **JOREK's kinetic neutral model** | **SOLPS** |
|---|---|---|
| Plasma | MHD equations | Fluid equations |
| Neutrals | Monte Carlo tracers | Equilibrium Monte Carlo tracers |
| Dynamics | Naturally time-dependent | Challenging |
| Drifts | $\mathbf{E} \times \mathbf{B}$ drift (can be switched off) | Challenging |
| Simulation time | $\sim$ 2 weeks for equilibrium (10ms/day) | $\sim$ 6 months |
| Maturity | Early (bugs, missing benchmarks) | Mature |
| Physics differences | - Single T | - $T_e$ & $T_i$ |
| | - Braginskii closure for $\kappa_\parallel$ in SOL | - Flux limiters |
| | | - Pumping |
| | | - Neutral collisions |
| | | - Molecular interactions |

included in JOREK, and there has not yet been a quantitative comparison of JOREK's kinetic neutral model against experiment nor a comparison of profiles (such as temperature as a function of major radius on the outer midplane) against SOLPS profiles. Although SOLPS has a fluid plasma model, which does not inherently include drifts, there is the possibility to include drifts. However, since the SOLPS run used for comparison did not have those drifts included, and it is challenging to set these simulations with drifts up, it was necessary to remove the evolution of electromagnetic variables from JOREK's MHD equations so as to switch of the naturally inherent $\mathbf{E} \times \mathbf{B}$ drift in JOREK by keeping $\mathbf{E} = \mathbf{0}$. Therefore a better benchmark would be to compare JOREK's kinetic neutral model against SOLPS simulations with drifts and reduced physics to match the physics of JOREK.

# Chapter 3:

# Improving and benchmarking JOREK's kinetic neutral model

In this chapter, the gap between JOREK's kinetic neutral model and reality is evaluated with aid of SOLPS (section 3.1), followed by the steps taken to close the gap (sections 3.2 - 3.4), and ended by an updated comparison to SOLPS (section 3.5) leading into the discussion of the remaining gap after the improvements (section 3.6).

## 3.1 Comparison of JOREK results to SOLPS at the start of the project

As mentioned in section 2.4.3, no comparison of profiles between kinetic neutral JOREK and SOLPS has been done before. Therefore the profiles from the runs in [4] have been compared against SOLPS simulations of the same ITER low performance scenario called PFPO-1, as published in [27], of which the data is made available on ITER's integrated modelling and analysis suite (IMAS). This scenario has a power of $P = 20$MW, plasma current $I_p = 5$MA, on axis magnetic field $B_0 = 1.8$T and no impurity seeding. Since these SOLPS runs were without drifts, JOREK's naturally present $\mathbf{E} \times \mathbf{B}$ drift has been switched off for all the runs shown in this chapter.

The comparison of 3 (lowest, medium and highest upstream densities of the two puff rate scans) of the profiles is shown in figure 3.1 at both the outer midplane and the inner and outer targets. At the outer midplane, the temperature tail of the JOREK profiles creeps up, signalling that energy is leaking in from the boundary into the SOL. Furthermore, the highest upstream density achieved for SOLPS is much lower than for JOREK, as for SOLPS it was difficult to increase the upstream density much above $n_{e,u} = 2 \cdot 10^{19}\mathrm{m}^{-3}$, which is the expected behaviour as once the SOL becomes fully detached, it is difficult to change the upstream density further by puffing more, precisely because the upstream and downstream quantities have become detached. The fact that this behaviour is not observed for JOREK signals that in JOREK it is more difficult to detach.

The same trend is observed from the target profiles. Both at the inner and outer targets, the highest upstream densities runs have negligible temperature for SOLPS but significant temperature for JOREK. Generally the target temperature in JOREK is larger than for SOLPS, showing that JOREK is not as detached. For low upstream density, the target density is lower for JOREK than for SOLPS showing that JOREK is still in the low recycling regime where SOLPS is already in the high recycling regime, and also the spread of the density at high upstream density is larger for SOLPS than for JOREK, meaning that there is more recycling at the far SOL in SOLPS than in JOREK, showing there that also the far SOL reaches the high recycling regime for lower upstream density in SOLPS than in JOREK. Finally the pressure of JOREK's medium upstream density is very comparable to SOLPS' low upstream density, and the pressure of JOREK's high upstream is somewhat in between SOLPS medium and high upstream density pressure profiles, even though the upstream pressures are similar for low and medium upstream densities. This again shows that there is more momentum loss in SOLPS than in JOREK for the same upstream density, signalling that JOREK is less detached than SOLPS.

The JOREK runs used here had puff rates of $\Phi_{low} = 88 \cdot 10^{21}$atoms/s, $\Phi_{medium} = 400 \cdot 10^{21}$atoms/s and $\Phi_{high} = 896 \cdot 10^{21}$atoms/s, whereas SOLPS only puffed $\Phi_{low} = 8.85 \cdot 10^{21}$atoms/s, $\Phi_{medium} = 70 \cdot 10^{21}$atoms/s and $\Phi_{high} = 200 \cdot 10^{21}$atoms/s, or in other words, SOLPS only needed a fraction of the puff rates necessary in JOREK to reach the same upstream densities. Actually the maximum fuel

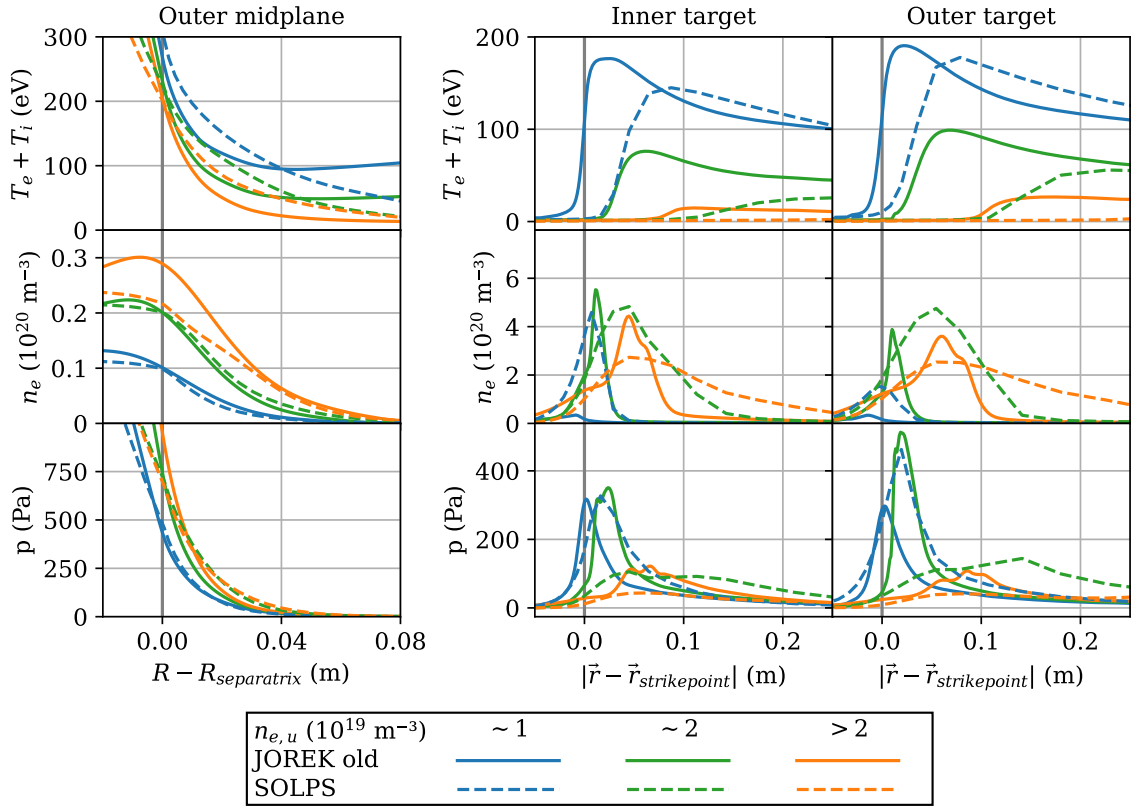


*Figure 3.1: Comparison of kinetic neutral JOREK results prior to this project (JOREK old; solid lines, results from [4]) to SOLPS results (dashed lines, results from [27]) for low (blue), medium (green) and highest (orange) upstream density of the respective puff rate scans. The x-axis for the targets is the physical distance to the strikepoint (where the separatrix hits the target) where a positive sign means at the SOL side, and a negative sign means at the PFR side of the separatrix. At the midplane, the density in the JOREK set could be pushed far above the highest achievable density in the SOLPS set, which signals difficulty to detach in JOREK. Furthermore, the temperature profiles are different, which is most apparent in the rising tails of JOREK (corresponding to the far SOL), which must mean there is energy leaking in from the far SOL. Although there are differences between JOREK and SOLPS at the midplane, limiting the validity of the comparison, profiles at the targets deviate more. JOREK's temperature is larger and peaks more closely to the separatrix. JOREK's density peaks in the PFR (left of strikepoint) for the lowest upstream density case (solid blue), and it is more peaked than SOLPS' profiles for the other cases. JOREK's pressure profiles seem to be a step behind SOLPS; JOREK's medium upstream density (solid green) corresponds quite well with SOLPS' low upstream density profile (dashed blue), while JOREK's highest upstream density corresponds better with SOLPS' medium upstream density profile (dashed green). This all suggest that given an upstream density, JOREK is not as detached as SOLPS, meaning the detachment behaviour in JOREK is lacking fidelity.*

throughput for ITER will be 200Pam$^3$/s with the possibility to double it for a short period of time [28]. For gas temperature of 100°C this corresponds to $\Phi_{ITER,max} = 2 \cdot 400[\text{Pam}^3/\text{s}]/(k_B \cdot 373[\text{K}]) = 155 \cdot 10^{21}$atoms/s where the 2 comes from the fact that there are 2 atoms in a $D_2$ molecule. This fuelling rate is much less than the required fuelling rate in JOREK to even reach medium upstream density, let alone high upstream density, thus something is ruining the particle balance in JOREK.

Where SOLPS is in a true steady state for these runs, as it is an equilibrium code, JOREK starts from a state far from equilibrium, and it is evolved over time until the SOL does not change anymore. This is not a true steady state but rather a quasi-steady state; the upstream density is constant and the target profiles have settled, meaning the SOL is in equilibrium, but nevertheless there is net particle transport to the core, and thus it is not a global equilibrium. This can be seen from the fact that for JOREK, the density profile at the outer midplane peaks near the separatrix rather than flattening out towards the core which would be the case for a global equilibrium. However, it is strange that there even is an equilibrium in the SOL, as there is no explicit pump implemented, thus in principle the particle content of the SOL should increase until the SOL would be filled completely with particles and all extra puffed particles would disappear in the core. This is not observed, so there must be some unintended numerical sink of particles in the SOL, which might cause all kinds of problems.

Besides the problems with JOREK mentioned above, the physics model in JOREK misses key elements as detailed in 2.4.3, which might explain some of the discrepancy. For example the separate ion and electrons temperature and molecular interactions both act as loss channels that help a SOL plasma to detach, and the neutral-neutral collisions are likely important to simulate recycling realistically as part of the recycling loop depends on the neutral flow, which is different for a colliding neutral gas compared to ballistic neutrals.

## 3.2 Improvements of JOREK's kinetic neutral model

In this section the improvements of JOREK's kinetic neutral model made during this project will be discussed.

### 3.2.1 Improving the energy transport in JOREK's kinetic neutral model

In plasma codes, an assumption must be done on what the turbulent transport is. The simplified equation for perpendicular heat flux is $q_\perp = \kappa \nabla_\perp T$. Usually, heat conductivity is determined as $\kappa_\perp = \chi_\perp n_e$ where the heat diffusivity $\chi_\perp \approx 1\text{m}^2/\text{s}$ is taken to be constant. This is for instance the case in SOLPS. However, in JOREK's main model $\kappa_\perp$ is taken as a constant value, which is fine for most applications of JOREK where only the core, which has roughly constant density, is of importance, however, for the current application the SOL is of importance, and in the SOL the density can span orders of magnitude, thus it makes sense to let the turbulent heat flux scale with the density. Therefore, an option was added to JOREK to let $\kappa_\perp$ depend on the normalised density $n_e/n_0$ where $n_0$ is the central density, the density in the core at the starting equilibrium. To avoid $\kappa_\perp$ from approaching 0, which could lead to numerical issues like negative temperature solutions, $\kappa_\perp$ was limited to be at least 1% of $\chi_\perp \cdot n_0$.

The rising tail in the temperature profiles at the midplane (see figure 3.1) was found to be caused by the sheath boundary condition acting as an energy source in the far SOL. On the targets, the sheath boundary condition is necessary to model the heat flux to the wall, but in the far SOL, there are parts where the magnetic field lines are parallel to the wall, and in that case the sheath boundary condition can behave unexpectedly and start acting as a large energy source or sink. Therefore, it was decided to use a Dirichlet boundary condition for the temperature in the far SOL. This was done by setting the desired temperature at the boundary for the initial profiles, and force the time evolution of the temperature at the boundary to be 0. The region where this Dirichlet condition was imposed could be chosen by specifying an interval in Z, so that the sheath boundary condition would stay imposed on the targets. This solution indeed removed the high temperature tail in the far SOL, while making sure

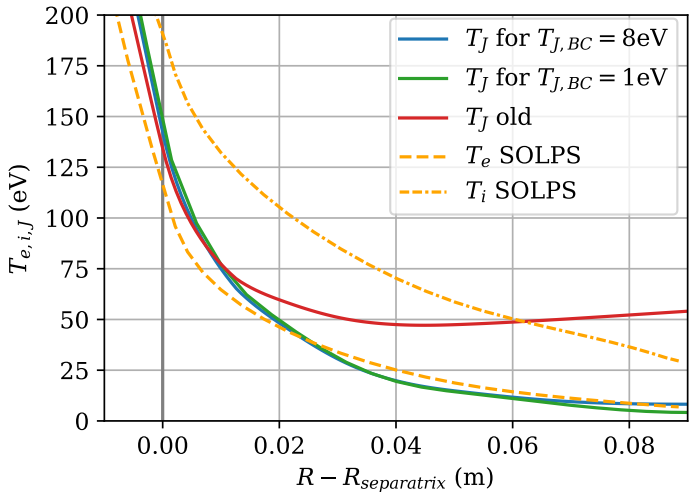


*Figure 3.2: Comparison of temperature profiles at the midplane to highlight improvements due to (1) making perpendicular heat conductivity $\kappa_\perp$ a function of density and (2) applying fixed temperature boundary condition in the far SOL. All upstream densities in this figure are $n_{e,u} \approx 1.0 \cdot 10^{19}\mathrm{m}^{-3}$. In the old scenario (red), JOREK's temperature $T_J$ would rise in the far SOL due to temperature leaking in at the sheath boundary condition at grazing angles, while after improvements (1) and (2), the profile is independent of the details of the boundary condition applied, as the $T_{J,BC} = 8\mathrm{eV}$ (blue) and $T_{J,BC} = 1\mathrm{eV}$ (green) scenario's have different fixed temperature boundary condition (and different Z interval, see text) but lead to the same solution in the relevant regime up to 7cm from the separatrix.*

that the near SOL profile was independent on the exact details of the boundary temperature chosen or the Z interval on which the Dirichlet boundary condition was imposed. The resulting profile due to these two improvements can be seen in figure 3.2, where the independence can also be seen. The Z interval where the Dirichlet temperature boundary condition was applied for the green curve was $0.5 < Z < 0.7$m, which is a thin region on the wall near the outer midplane, whereas the interval for the blue curve was $-2.5 < Z < 4.06$m, which is all of the far SOL excluding the top of the device where some of the field lines starting at the target end up. All future JOREK runs in this document use the latter interval.

### 3.2.2 Improving the particle balance in JOREK's kinetic neutral model

As mentioned in section 3.1, unrealistically large puff rates were needed in JOREK, and then still it was surprising that a quasi steady state was reached as no pump was implemented. Both of these facts point to particles being unintentionally lost from the simulation. Remember from section 2.1 that recycling plays an important role in going from an attached to a detached state, and to model recycling well, a single particle must appear many times in the flux to the wall. This means that a small undesired particle loss can significantly change the detachment behaviour. Therefore it is crucial to solve these unintentional particle losses. In this section, it will be discussed where these particles were getting lost, and how those problems are solved.

There were three separate problems identified causing particles to disappear within the thousands of lines of JOREK's kinetic neutral model:

1. The most important factor was that the ions lost at the wall were not exactly compensated by neutrals generated at the wall, because the recycling integral on the neutrals part had terms missing compared to the plasma part. The neutral recycling flux was calculated as

$$\Gamma_{i,calc} = n_e c_s \cos\alpha \tag{3.1}$$

where $c_s$ ion sound speed at the wall, and $\alpha$ is the angle between the wall normal and the magnetic field. The plasma on the other hand had a flux onto the wall of

$$\Gamma_{i,plasma} = n_e \mathbf{v}_{\parallel} \cdot \mathbf{n} + n_e c_s \cos 89^\circ \tag{3.2}$$

where $\mathbf{v}_{\parallel}$ is the parallel velocity at the target, which is approximately equal to $c_s$, and the term $n_e c_s \cos 89^\circ \approx n_e c_s 0.017$ is an imposed dissipation term that is always present but is dominant for grazing magnetic field lines, with the purpose to model perpendicular diffusion so that there is no unphysical density build-up at regions where the field line grazes the wall, i.e. where $\mathbf{v}_{\parallel} \cdot \mathbf{n} \to 0$, such as around the dome in the PFR. This dissipation term is not negligible at the targets where $\mathbf{b} \cdot \mathbf{n} \approx 0.04$. The solution was to add the relevant terms to the flux integral on the neutral side of the code so that the right amount of neutrals would be generated.

2. The second problem was that neutral super-particles did not always correctly reflect off the wall upon hitting the wall. There was an indexing error in a subroutine which figured out in which boundary element the super-particle had hit the wall, which meant that sometimes the wrong boundary element would be returned. This caused some super-particles, and the weight they represented, to be lost from the simulation. The solution was to fix the indexing subroutine so that always the right boundary element would be returned.
3. The third issue was that in the code there was a separation between super-particles hitting the wall and them being reflected back into the domain. During this waiting, they were not recognised as active super-particles. There happened to be a recombination routine in this part of the code which needed to initialise new particles. However, this recombination routine did not recognise the to-be-reflected particles as such, and thus when a new super-particle needed to be initialized, this could overwrite such a to-be-reflected super-particle, essentially deleting the atoms represented by that super-particle. The solution for the scope of this project was to move the routine which handles the reflections in front of the recombination routine, such that no overwriting of particles could happen anymore.

With these improvements, the total particle content, i.e. the integral of all atoms in the simulation from both the plasma and the neutrals, is conserved up to ∼3% of the puff rate compared to errors of ∼100% prior to the project. See figure 3.3 for comparison before and after the improvements made, where the expected change in content from $t = 0$ is simply the integral over the puff rate $\int \Phi \mathrm{d}t$ for these simulations, as there is no pumping or other intentional particle sink. The remaining error in the particle content could be due to the finite element approximation which makes it difficult to know the exact ion flux onto the wall, and given the large integral over the ion flux compared to the puff rate, a small error in the ion flux calculation to generate recycled neutrals will already be visible in the particle content. To test this hypothesis, the element size could be made smaller, and to solve this issue better, a correction on the calculated recycling flux based on the change in simulated plasma content could be made, although this may not be desirable as no information on the location of the lost particles is known. However for the current project, the error of a few percent is not considered a large issue, and thus the confirmation and possible solutions to the root cause of the remaining error are left for future work.

## 3.3 State of JOREK after improvements

After the improvements discussed in the previous chapter, JOREK's kinetic neutral model can reach detachment for realistic ITER puff rates. In figure 3.4, the results of a simulation with constant puff rate of $\Phi = 100 \cdot 10^{21}$atoms/s are shown. Since the remaining error in the total particle content is small compared to the puff rate, the total content increases over time and thus the SOL does not reach equilibrium, which can be seen by the decay of the temperature on the inner target and the steady rise of recycling and recombination rates. The large recycling and ionisation rates compared to the puff

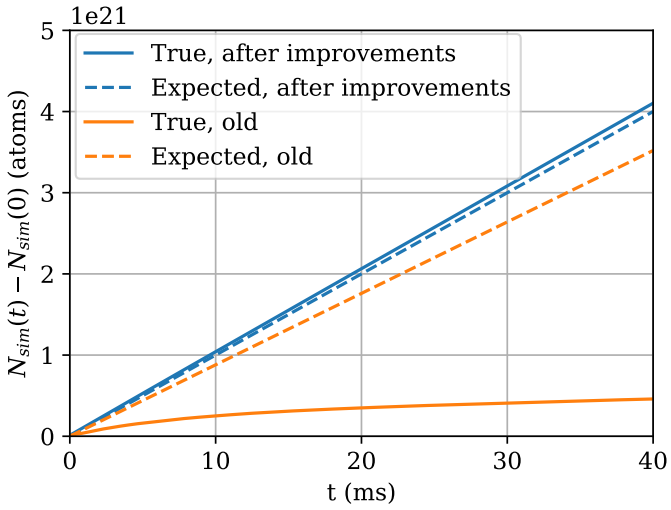


*Figure 3.3: The true change of atom content (neutrals + plasma atoms) in the simulation compared to what is expected, i.e. $\int \Phi \mathrm{dt}$. Previously (orange), the true content was significantly lower than expected and it flattened over time, meaning atoms were lost on the order of the puff rate. After removing unintentional particle sinks, the true atom content follows the expected content with an error in the order of $\Phi = 3 \cdot 10^{21} \mathrm{atoms/s}$ compared to the puff rate of $\Phi = 100 \cdot 10^{21} \mathrm{atoms/s}$. This remaining error is likely due to the finite element approximation which does not conserve particles fully.*

rate shows that the SOL is in the high recycling regime, while the small (compared to the recycling rate) but growing recombination rate shows the SOL state is approaching detachment but is not there yet. Thus, reaching equilibrium in JOREK will now require the intentional removal of particles from the SOL by pumping particles, which will be discussed in the next section.

## 3.4 Moving JOREK simulation into the relevant SOL regime: steady state

Both for the comparison against SOLPS, and for studying the dynamics, it is desirable to have an equilibrium JOREK simulation. As was seen in the previous section, due to the improvements in the particle balance it now has become necessary to intentionally pump to be able to reach a steady state with JOREK's kinetic neutral model.

Therefore in this section it will be described how a pump was added to JOREK's kinetic neutral model, and how a global near steady state regime was reached with this implemented pump.

### 3.4.1 Physical relevance of pumping with finite neutral absorption

As there are no neutral-neutral collisions yet in JOREK's kinetic neutral model, any pump implemented in JOREK will currently be a simplistic approximation of reality. Therefore it was chosen to implement the pumping in JOREK by having a finite absorption coefficient at a section of the domain boundary in the PFR. This is a simple solution to implement, the physics principle behind it is reasonable and it is widely used in for example SOLPS. The physics principle of using a finite absorption coefficient is that in the ITER pumping system, there will be a cold trap, i.e. an area which absorbs gas particles by freezing them onto a cryogenic surface [24]. This cold trap will be some distance away from the pump entrance in the vacuum vessel, and thus there will be a finite pressure inside the pump duct, meaning that a virtual interface could be defined where there are particle fluxes in both directions with

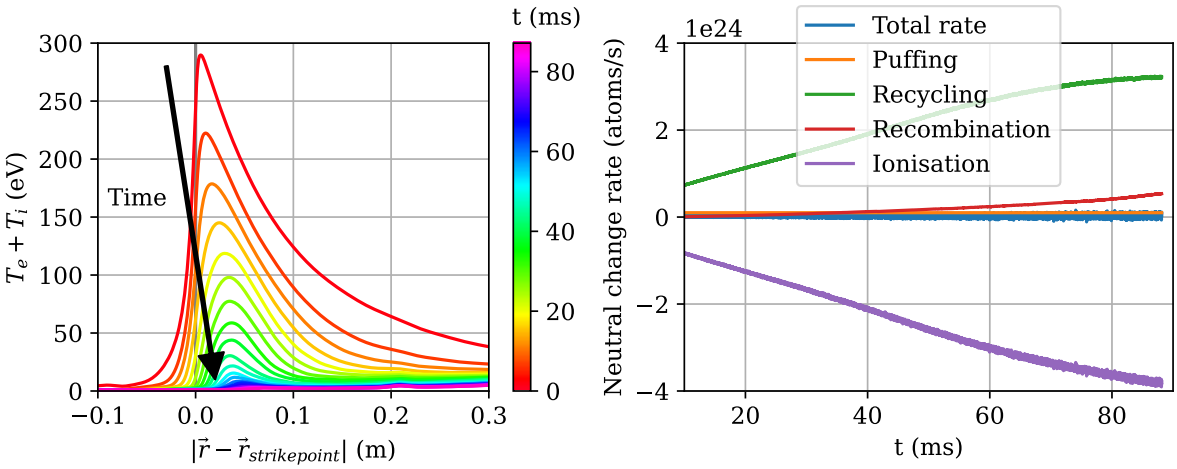


*Figure 3.4: Results of simulation with constant gas puff of $\Phi = 100 \cdot 10^{21}$atoms/s after the particle conservation improvements (see section 3.2). Left: Temperature evolution at the inner target. Since particles are conserved and there is no pump, the SOL progressively detaches over time due to the build-up of high plasma density near the targets, thus lowering the temperature. Right: Neutral particle balance. As can be seen and is typical for highly recycling scenario's, the gas puff (orange) is small (factor $1/30$) compared to the recycling flux (green), and the recycling almost fully compensates ionisation (purple). Furthermore, the bulk recombination (red) grows, while the recycling rate (green) stagnates, which shows that the SOL state is moving to detachment. At the end, the neutral rates have not settled to an equilibrium value yet, and thus longer simulation would see the SOL detaching further. Therefore, the time evolution of both figures clearly shows that in this one run, the SOL moves from an attached to a the beginning of a detaching state without reaching equilibrium.*

a net flux into the pump duct. This can be modelled by having incoming particles be absorbed at this virtual interface with finite absorption coefficient. When neutral pressure is resolved, the absorption coefficient can be linked to the pumping speed $c_p(\mathrm{m}^3/\mathrm{s})$ at the pump entrance with [29]

$$c_p = 3.9 \cdot 10^3 \xi S \sqrt{\frac{T_{eV}}{A}} \tag{3.3}$$

where $\xi$ is the absorption coefficient, $S(\mathrm{m}^2)$ is the area of the pump, $T_{eV}(\mathrm{eV})$ is the temperature of the gas at the pump entrance, and $A$ is the atomic mass number. Given pump area of $S = 12.6\mathrm{m}^2$ (see section 3.4.2) for engineering pumping speed $c_p = 75\mathrm{m}^2/\mathrm{s}$ [24] at room temperature $T_{eV} = 0.025\mathrm{eV}$ for deuterium with mass number $A = 2$, the resulting absorption coefficient would be $\xi = 1.4\%$. For JOREK however, far larger absorption coefficients will be necessary to reach equilibrium (see section 3.4.3), as the lack of neutral-neutral collisions in the model means that the neutral gas, which has a large density in the PFR, does not expand against the wall as much as it physically should.

### 3.4.2 Implementation of pumping in JOREK

The pumping is implemented in JOREK by specifying at which boundary elements to pump, and what absorption coefficient should be used. The chosen boundary elements corresponded to two separate areas on the dome as shown in figure 3.5, as that is approximately where the PFR connects to the area under the dome in ITER, with total area $S = 12.6\mathrm{m}^2$.

In the module which handles reflections, the weight of super-particles reflected on the specified elements is adjusted with $W_{new} = W_{old} \cdot (1 - \xi)$. This change in weight from pumping is summed over an MHD time step and printed to the output file as diagnostic of the global pumping rate $\Phi_{pump}$. In figure 3.6, it is shown that the particle balance is still conserved well, with the expected content

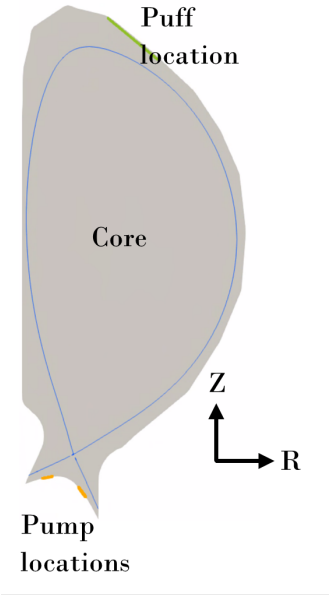


*Figure 3.5: Location of pumping and puffing. The pumping is implemented by having a nonzero absorption coefficient at the finite elements marked with orange. For the pumped equilibrium runs the puff location was on the separatrix rather than on the top of the device, to help kick start the recycling without increasing the upstream density.*

including the pump being the content at $t = 0$ plus $\int \Phi_{puff} - \Phi_{pump} \mathrm{dt}$. The error is $3 \cdot 10^{21}$atoms/s, which is the same as before and now about 5% of the puff rate of $70 \cdot 10^{21}$atoms/s.

### 3.4.3 Reaching global near steady state in JOREK

As JOREK is inherently time dependent, reaching a global steady state requires letting the simulation run for long enough that everything ends up in equilibrium. When starting far away from equilibrium, this would take multiple confinement times ($O(10\mathrm{s})$, which would take years to simulate (at 10 ms/day). Instead the starting state is chosen to be as close to equilibrium as possible, so that a state close to global equilibrium, called global near steady state (GNSS), is reached on the order of weeks. To have global particle equilibrium means that the pumping plus numerical losses must equal the puffing, and since the core evolves slowly, the initial state must have an equilibrium combination of puff rate, absorption coefficient and core density. As the absorption coefficient loses its physical meaning in absence of neutral-neutral collisions (section 3.4.1), it was chosen to use this as a tuning parameter, where the puff rate and core density could be taken from SOLPS simulations. Note that SOLPS does not have to wait for the full core to evolve as they use a boundary condition just inside the separatrix for the core. This boundary condition for the core could in principle be implemented for JOREK in the future too in order to generate equilibria from scratch, however first the neutral-neutral collisions would need to be added to have physically reasonable pumping.

Given that the SOL must be kept in the semi-detached state, the relevant dynamics for control are those near the semi-detached state, thus for the global equilibrium, it was chosen to recreate SOLPS' medium upstream density scenario, where $n_{e,u} = 2.0 \cdot 10^{19}\mathrm{m}^{-3}$, which corresponded to a core density of $n_{e,core} = 2.2 \cdot 10^{19}\mathrm{m}^{-3}$ and puff rate of $\Phi = 70 \cdot 10^{21}$atoms/s. An initial equilibrium was generated for this core density, which was then evolved using the given puff rate for a scan of absorption coefficients. Since initially there are no neutrals in the SOL, first the upstream density will fall as the plasma fills the SOL, after which the puffed neutrals will compensate for this, pushing the upstream density back up. For perfect equilibrium values, the upstream density would be perfectly pushed up asymptotically over time. It was found that the absorption coefficient $\xi = 50\%$ performed better than $\xi = 10\%$,

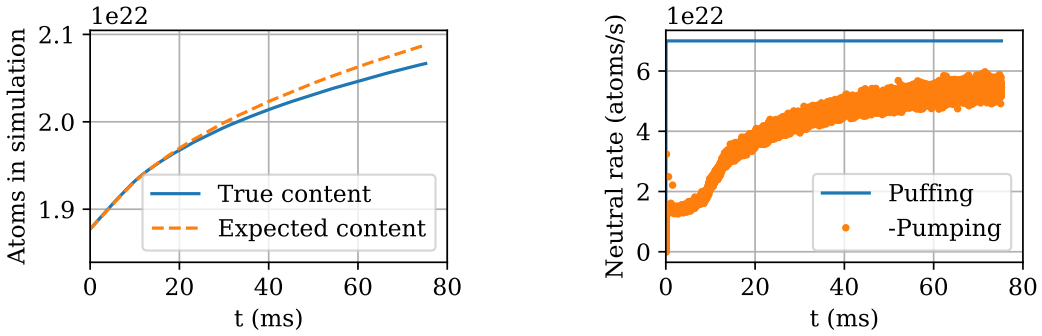


*Figure 3.6: Total particle balance (left) and comparison of puff rate to pump rate (right) for global near steady state run. The total particle content shows that with pumping, simulation particle content is still conserved well. The error is still* $3 \cdot 10^{21}$atoms/s *which is about 5% of the puff rate of* $70 \cdot 10^{21}$atoms/s. *Although the slope of the total particle content flattens due to the increase in pumping over the simulation (right), the total content still increases even after* 70ms*, meaning the simulation is not truly steady state. Comparison of puff rate to pump rate (right) show that as time progresses, the pump rate approaches the puff rate as the pump becomes more efficient for higher PFR neutral density. Here again, the pump rate after* 70ms *is not yet equal to the puff rate, also not when the numerical particle loss of* $3 \cdot 10^{21}$atoms/s *is taken into account.*

which overshot the correct upstream density faster, and $\xi = 99\%$, which did not recover the correct upstream density within the 45 ms simulation. The resulting equilibrium is not a perfect equilibrium, as the total particle content increases (figure 3.6, left). This is the result of the puff rate being larger than the pump rate (figure 3.6, right). This is true also when the error of the total particle content of $3 \cdot 10^{21}$atoms/s is taken into account as loss term. This net puffing effect results in the upstream density slowly overshooting the equilibrium as can be seen in figure 3.7. Nevertheless, the target profiles are stable from about halfway the simulation, thus this state can be considered a reasonable approximation of steady state, i.e. GNSS.

## 3.5 Benchmark of JOREK against SOLPS after improvements

After all the improvements mentioned in the previous three sections, a new benchmark against SOLPS was performed which can be seen in figure 3.8. The GNSS run is included, but also specific time stamps of the transient $\Phi = 100 \cdot 10^{21}$atoms/s run without pumping (described in section 3.3) are compared to both initial JOREK's kinetic neutral results and to SOLPS. The GNSS run has lower upstream temperature than all other runs as the initial equilibrium had a higher core density than the other JOREK runs, so by lack of a physical argument to allow the core pressure to be raised, the upstream temperature is lower in the GNSS than in the other runs. Upon further investigation, the core temperature profile in SOLPS approached the GNSS core temperature profile, rather than the higher core temperatures in the other JOREK runs, which turned out to be caused by the core temperature profile in JOREK not to be in equilibrium, as for instance the temperature profile on the magnetic axis visibly evolved within the $<$ 100ms of simulated time, which should not be possible with energy confinement time on the order of seconds. Depending on the details of the simulation, on the order of 2MW of net power could flow into or out of the core, compared to the 20MW of heating power. Although this adds to the global equilibrium of the GNSS not being a true equilibrium, this issue is expected to be small compared to the missing physics of JOREK, and thus left as future work.

As becomes clear from the comparison, the results of the transient run are closer to SOLPS than the runs prior to this project, while results of the GNSS run are further away from SOLPS results than both the transient and the old runs. Since the GNSS is the best comparison to SOLPS, this leads to the conclusion that JOREK's kinetic neutral model, although improved in this project, still misses

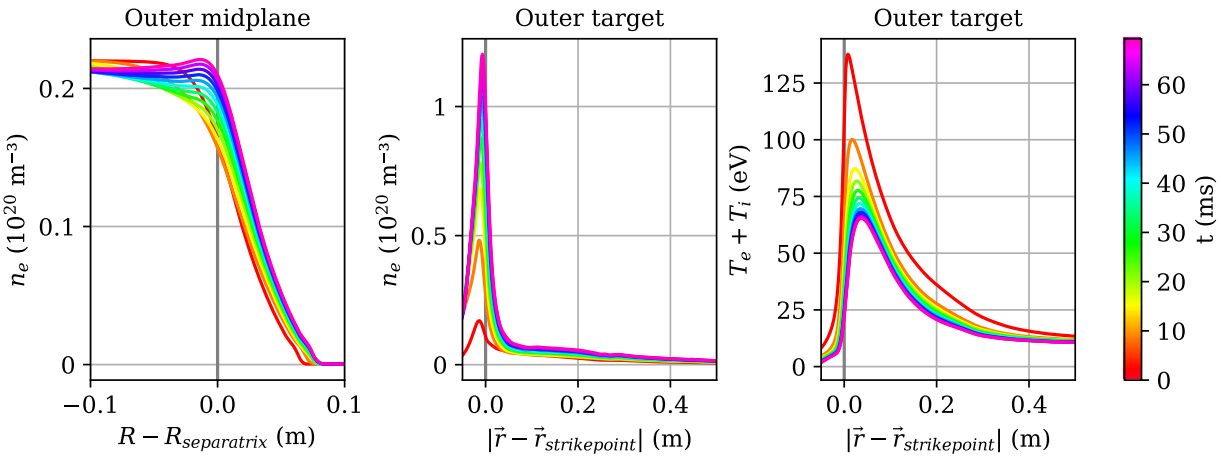


*Figure 3.7: Global near steady state run time evolution without drifts. Using puff rate* $70 \cdot 10^{21}$atoms/s *and core density* $n_{e,core} = 2.2 \cdot 10^{20}\mathrm{m}^{-3}$*, it was found that an absorption coefficient of 50% keeps the upstream density nearly constant after initial settling, as can be seen by the fact that the profile at the latest time step (purple) in the upstream density figure (left) is close to the desired core density and to the time steps just before it (blue). The profiles on the targets (here only the outer target is shown for brevity; middle and right figure), are also nearly constant from* $t = 40$ms *(cyan) onwards, thus this SOL state can be considered a global near steady state.*

key physics to model the SOL reliably and thus cannot be used in the current state to produce high fidelity control results.

## 3.6 Remaining gap in JOREK's SOL physics model

Although significant improvements to JOREK's kinetic neutral model have been achieved in the current work, there still is a non-negligible difference between JOREK's kinetic neutral model and SOLPS. The remaining known discrepancies between JOREK's kinetic neutral model and reality are:

1. The lack of neutral-neutral collisions, which affects both how realistic the pump can be, and it might significantly influence the recycling cycle which is known to be important for detachment behaviour.
2. The lack of molecules, and thus the lack of molecular interactions and loss channels. Molecules play an important role in the energy and momentum loss channels available in the plasma and thus can significantly influence the detachment behaviour.
3. The single temperature model. Rather than having separate and thus more refined loss channels for both the electrons and ions, JOREK's kinetic neutral model currently simplifies the physics. This might be important but is expected to be less important than 1 and 2.
4. Equilibrium core temperature. As mentioned in the previous section, the core temperature profile in the JOREK runs shown in this work were not in equilibrium, which changes the SOL behaviour, albeit it not expected to be a major cause of the model's low fidelity.
5. Flux limiters for the SOL. Currently JOREK's kinetic neutral model uses the Braginskii closure to model parallel heat conductivity $\kappa_\parallel$, which is known to be a bad approximation in the SOL. Since heat flux to the targets plays an important role in the detachment behaviour, this might cause a significant discrepancy.
6. Remaining error in total particle content. As discussed in section 3.2, a remaining error of $\Phi = 3 \cdot 10^{21}$atoms/s is seen in the total particle content, which is not large but also not negligible,

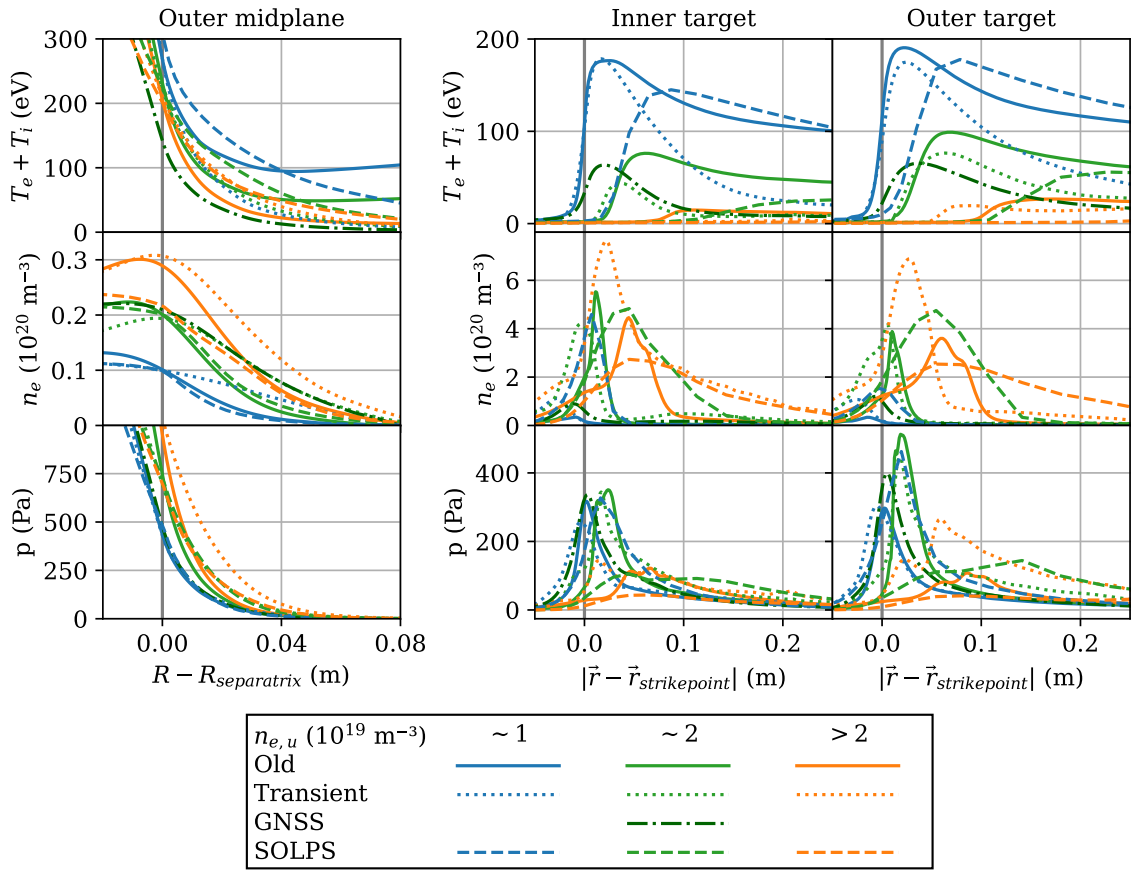


*Figure 3.8: Comparison of different versions of JOREK's kinetic neutral model, prior to this project (old), after improvements but without pump (transient) and global near steady state (GNSS), to SOLPS, for low (blue), medium (green) and high (orange) upstream densities, except for the GNSS, which was only available for the medium upstream density. Due to the renewed equilibrium of the GNSS to have higher core density, the upstream temperature profile is lower than all other simulations as pressure in the equilibrium is conserved, limiting its comparison to the rest. On the targets it can be seen that the transient run performs closer to SOLPS than the old runs, but is still significantly off, while the GNSS run performs similar in target temperature (which is somewhat deceiving given the lower upstream temperature) but worse in target density and pressure than both the transient and the old JOREK medium $n_{e,u}$ runs. This can be explained from the fact that the density does not build up as efficiently compared to the other JOREK runs since (1.) the puff rate is lower than all old JOREK runs and the transient run, and (2.) neutrals easily escape into the PFR as there are no neutral-neutral collisions, and there they are pumped. Since the GNSS run, which is the closest comparison to SOLPS yet, is still significantly different, it must be concluded that the underlying physics model simplifications in JOREK do not represent reality well enough, and thus JOREK's results cannot currently be trusted to produce reasonable control related results. Therefore the rest of this work aims to prepare for the control analysis and do a proof of concept, so that once the physics model in JOREK's kinetic neutral model is improved, it will be easy to repeat the analysis to produce high fidelity control results.*

especially for lower puff rates.

7. Remaining error in neutral particle balance. Since all terms in the neutral particle balance are known up to machine precision, the difference between the sum of the individual terms and the measured change of the sum of super-particle weight, i.e. the error in the neutral particle balance, should be of order machine accuracy of the sum of all weights. It turns out this error is larger, and although very small and negligible by itself, this could point to a bug with more significant consequences.
8. Possible issue with super-particles being stuck at the wall during reflections. It was observed that super-particles sometimes seemed to stay at the wall without being correctly re-emitted into the domain. This seemed to have to do with the the angle of reflection sometimes being negative. Further investigation would be necessary into the cause and whether this could generate any issues in the simulation.
9. Crashes during the simulation might point to underlying problem. The simulations tended to crash often, and often without clear origin. Initially a lot of crashes seemed related to either oscillations in parallel velocity or to negative temperatures or densities, but after these profiles were numerically smoothed to avoid these issues, there were still crashes with unknown origin. This might point to a problem in the physics model, or might be a purely numerical phenomenon.

Although it will require the necessary effort, all of these potential issues can be overcome. The focus should be on the first two issues as these are known to be important players in modelling the physics correctly.

Given the differences between the GNSS and SOLPS, and the control scope of this work, the rest of this work will prepare the analysis routine with which the desired control quantities; the timescales, the relation between SOL current and peak heat flux, and the system's transfer function, can be determined. In that way, once the physics reliability of JOREK's kinetic neutral model has improved, the analysis routine can be re-used to produce high fidelity control results. After setting the analysis routine up (chapter 4), the analysis will be applied on transient runs starting from a GNSS with drifts to prove the concept of the analysis routine and produce an initial low fidelity first insight into the control quantities (chapter 5).

# Chapter 4:
# Preparing for dynamic studies

This chapter contains the preparations necessary for obtaining the control related quantities from kinetic neutral JOREK. First the method to extract the SOL current from JOREK simulations will be discussed, followed by the preparation for acquiring a SOL system transfer function.

## 4.1 Extracting SOL currents from JOREK simulations

This section describes why and how the SOL current is determined for JOREK using a post-processing routine. First the motivation to post-process, and the equation will be discussed, followed by the timescale in which the SOL current develops and ended by the implementation into JOREK and the benchmark of the routine.

### 4.1.1 How to model SOL current in JOREK

The SOL current can either be determined consistently by incorporating the right boundary conditions in JOREK, or it can be post-processed using an equation. The sheath boundary condition in JOREK does not model the sheath potential itself but only the resulting heat fluxes. Since positive currents to a target cannot exceed saturation current density, the resulting sheath boundary condition is nonlinear, making it difficult to work with and simulate. Although this is theoretically possible and should be pursued in future work, due to the control scope of the current work, the easier method of determining the SOL current from an equation will be used. This means the SOL current is not self consistent with the plasma state.

Since the SOL current is of order 10kA (see figure 4.1), while the plasma current is $I_p = 5$MA in PFPO-1, the magnetic equilibrium is not affected much. However, post-processing the SOL current also assumes that the SOL current is in equilibrium for a given SOL state, meaning that the timescale in which the SOL current responds to changes in the SOL state must be much faster than the timescales in which the SOL state changes. This turns out not to be a valid assumption in all cases as shown in the next section. Nevertheless, since the boundary condition is out of scope, the SOL current will be determined through post-processing.

The equation used to determine the SOL current density is given in [17], equation 17.29:

$$\hat{j}_\parallel = -\gamma \left[ \frac{eV_0}{kT_h} + \left( \frac{1}{r_T} - 1 \right) (\ln 2 - 0.71 + \ln \alpha) + \ln \left[ \frac{1 + \hat{j}_\parallel}{(1 - r_n r_T^{1/2} \hat{j}_\parallel)^{1/r_T}} \right] - \frac{1}{kT_h} \int_h^c \frac{1}{n} \frac{\mathrm{d}p_e}{\mathrm{d}s_\parallel} \mathrm{d}s_\parallel \right] \quad (4.1)$$

Here the first term in the brackets relates to the external bias difference $V_0 = V_c - V_h$ applied between the hot and cold sides of the plasma, which for the current work is $V_0 = 0$V. The second term represents the thermoelectric effect (the difference in sheath potentials at the two targets) explained in section 2.1.1, and is usually the dominant term. The third term represents the fact that the current density is limited by the saturation current density, as when $\hat{j}_\parallel$ becomes of order 1, this term limits $\hat{j}_\parallel$. The last term represents current driven by a pressure gradient along the fieldline and it's contribution is most prominent in the PFR.

In the equation, $k$ is the Boltzmann constant, $r_T = T_h/T_c$ the temperature ratio, with subscripts $h$ and $c$ meaning the hot or cold side of the fieldline, $\alpha = 1/2(m_i/\pi m_e)^{0.5}$ is a numerical factor containing the electron $m_e$ and ion masses $m_i$, $r_n = n_h/n_c$ is the density ratio, and $p_e$ is the local pressure, with

$s_\parallel$ the direction along the fieldline from the hot to the cold side. The normalised current density is given by

$$\hat{j}_\parallel = \frac{j_\parallel}{e n_h c_{sh}} \tag{4.2}$$

with parallel current density $j_\parallel$, electric charge $e$, and ion sound speed at the hot target

$$c_{sh} = \sqrt{\frac{2kT_h}{m_i}} \tag{4.3}$$

The factor in front of equation 4.1 is

$$\gamma = \frac{\sigma_{\parallel,av} \cdot kT_h}{e^2 L n_h c_{sh}} \tag{4.4}$$

with $L$ the connection length between the targets and where the flux average conductivity is given by ([30] equation 2):

$$\sigma_{\parallel,av} = \frac{e^2 \lambda_{11} L}{m_e} \left[ \int_h^c \frac{\mathrm{d}s_\parallel}{n_e \tau_{ei}} \right]^{-1} \tag{4.5}$$

where $\lambda_{11} = 1.975$ is a Spitzer-Härm coefficient, with the value corresponding to charge $Z_i = 1$ [31], and $\tau_{ei}$ is the electron-ion collisions time, which is the inverse of the collision frequency $\nu_{ei}$ given by ([17] equation 9.23):

$$\tau_{ei}^{-1} = \nu_{ei} = \frac{0.51 e^4 \ln\Lambda Z_i n_e}{3 m_e^{1/2} \varepsilon_0^2 (2\pi k T_e)^{3/2}} \tag{4.6}$$

with vacuum permittivity $\varepsilon_0$ and Coulomb logarithm $\ln\Lambda$, which for $Z_i = 1$ is calculated according to [32]

$$\ln\Lambda = \begin{cases} 23 - 0.5\ln\left(n_{e,\mathrm{cm}^3}\right) + 1.5\ln\left(T_{e,\mathrm{eV}}\right), & \text{if } T_{e,\mathrm{eV}} < 10\mathrm{eV} \\ 24.1513 - 0.5\ln\left(n_{e,\mathrm{cm}^3}\right) + \ln\left(T_{e,\mathrm{eV}}\right), & \text{otherwise} \end{cases}$$

where $n_{e,\mathrm{cm}^3}$ is the electron density in $\mathrm{cm}^{-3}$ and $T_{e,\mathrm{eV}}$ is the electron temperature in eV.

In the analysis resulting in equation 4.1 discussed in [17], it was assumed that the magnetic geometry was slab geometry, and that $\sigma_\perp = 0$ such that the thermoelectric current density is parallel to the magnetic field.

In reality the thermoelectric current might have a perpendicular component. An upper limit of the perpendicular current can be found from the pressure balance in equilibrium

$$\mathbf{j} \times \mathbf{B} = \nabla p \rightarrow j_\perp B = |\nabla p| \tag{4.7}$$

with $\mathbf{j}$ total current density, $j_\perp$ the current density perpendicular to the magnetic field $\mathbf{B}$, and $p$ the total plasma pressure. Although there can be other contributions to $\mathbf{j}$, the thermoelectric contribution $j_{\perp,SOL}$ is likely not much larger than $j_\perp$. Approximating the gradient of the pressure at the separatrix as the pressure $p_{sep}$ over the SOL decay length $\lambda_{SOL}$, we find

$$j_{\perp,SOL} \lesssim j_\perp = \frac{\nabla p \times \mathbf{B}}{B^2} \approx \frac{p_{sep}}{d_{SOL} B} \tag{4.8}$$

which for the end of the transient run (see figure 3.8 orange dotted line) with $p_{sep} = 1\mathrm{kPa}$, $\lambda_{SOL} = 2\mathrm{cm}$ and $B = 1.8\mathrm{T}$ gives $j_{\perp,SOL} \leq 28\mathrm{kA/m}^2$, which is small compared to the current density peak calculated of around $j_{SOL} = 180\mathrm{kA/m}^2$ seen in figure 4.1, albeit not negligible.

Thus the current must flow predominantly along the fieldlines; $\mathbf{j} \approx j_\parallel \mathbf{B}/|B|$. Since equilibrium currents are divergence free $\nabla \cdot \mathbf{j} = \mathbf{0}$ (i.e. quasi-neutrality), we get

$$\nabla \cdot \mathbf{j} = \nabla \cdot (\mathbf{B} j_\parallel / |B|) = j_\parallel / |B| \nabla \cdot \mathbf{B} + \mathbf{B} \cdot \nabla (j_\parallel / |B|) = \mathbf{B} \cdot \nabla (j_\parallel / |B|) = 0 \tag{4.9}$$

where we used the product rule for divergence and Maxwell's $\nabla \cdot \mathbf{B} = 0$. This means that $j_\parallel/|B|$ is the flux function, and given that the magnetic field is dominated by the toroidal field $|B| \approx B_\phi = F_0/R$

which scales with the inverse of the major radius, the current density along the field scales with $1/R$ too. Thus in the rest of this work, $j_\parallel$ is taken to mean the current density at average radius between the two targets $R_{av} = 5.0$m, such that the current onto the wall at either targets is given by

$$|j_{wall}| = |j_\parallel (R_{av}/R)\mathbf{B} \cdot \mathbf{n}_{wall}| \tag{4.10}$$

where $\mathbf{n}_{wall}$ is the normal vector to the wall and the sign of $j_{wall}$ is such that it is positive for current into the wall.

### 4.1.2 SOL current self induction timescale

To deduce the SOL current response timescale, consider the SOL with continuous and overlapping resistance and inductance as an $\mathcal{R}L$ circuit with separate resistor $\mathcal{R}$ and inductor $L$ in series. Since it is a circuit in series, the current $I$ is the same in both components and the total voltage difference over the circuit $V$ is the sum of the two components,

$$V = V_L + V_R = L\frac{\mathrm{d}I}{\mathrm{d}t} + I\mathcal{R} \tag{4.11}$$

Where we used the definition of inductance $L$. Rewriting this as a differential equation for $I$ we get

$$\frac{\mathrm{d}I}{\mathrm{d}t} + \frac{\mathcal{R}}{L}I = \frac{V}{L} \tag{4.12}$$

which has solution

$$I(t) = \frac{V}{\mathcal{R}}\left(1 - e^{-t\mathcal{R}/L}\right) \tag{4.13}$$

which means the characteristic response time of the system is $\tau := L/\mathcal{R}$.

Modelling the SOL as a toroidal current loop in which the current only flows on the surface of the wire, the resistance is

$$\mathcal{R} = \frac{l}{\sigma A} \approx \frac{2\pi R}{\sigma 2\pi a\kappa d_{SOL}} = \frac{R}{\sigma a\kappa d_{SOL}} \tag{4.14}$$

where $l$ is the toroidal length, $A$ the poloidal cross sectional area in which the current flows, $R$ the major radius, $\sigma$ the conductivity in the SOL, $a$ minor radius with $\kappa$ the elongation, and $d_{SOL}$ the thickness of the SOL in which the current flows.

The inductance of a current wire is given by [33]

$$L \approx \mu_0 R\left[\ln\left(\frac{8R}{a}\right) - 2 + \frac{Y}{2}\right] \tag{4.15}$$

where $\mu_0$ is vacuum permeability, $R$ is the radius of the wire loop, which is equal to the major radius of the tokamak, $a$ is the wire thickness, which is equal to the minor radius of the tokamak, and $Y$ describes the internal inductance within the wire, with $Y = 0$ for current carried exclusively at the surface of the wire.

Thus the characteristic timescale in which the scrape-off layer current develops is

$$\tau = \frac{L}{\mathcal{R}} = \mu_0 \sigma a\kappa d_{SOL}\left[\ln\left(\frac{8R}{a}\right) - 2\right] \tag{4.16}$$

where $\sigma = 1 \cdot 10^6 \Omega^{-1}\mathrm{m}^{-1}$ (see figure 4.1), $R = 6.2$m, $a = 2.0$m, $\kappa = 1.5$, and from the width of the $j_{wall}$ profile at the targets (see figure 4.1), it is found that $d_{SOL} \approx 0.03$m at the OMP, resulting in $\tau = 0.14\mathrm{s} = 140\mathrm{ms}$.

Note that this timescale scales as $\tau \sim \sigma a d_{SOL}$ so it is longer for ITER than for smaller devices such as AUG. Therefore this result does not contradict measurements of current day devices such as in AUG shown in ([13] figure 1).

Additional effects not taken into account in the above calculation include $Z_{eff} > 1$, which increases $\mathcal{R}$, and the conducting vacuum vessel, which effectively lowers $L$ [34], and neoclassical electron trapping (i.e. banana orbits) which increases $\mathcal{R}$. In addition, the current density is limited by saturation $j \leq j_{sat}$. This generates a sheath resistance which increases the total resistance $\mathcal{R}$. Therefore the true self-induction timescale is likely lower than the above approximation of 140ms, thus whenever the rest of the report quotes $\sim$ 0.1s as initial estimate for the self-induction timescale, remember that this is likely an overestimate.

Nevertheless, since it takes a few $\tau$ to reach equilibrium, the SOL current will likely not be in equilibrium during the fast changes of the SOL observed in the simulations (see chapter 5), and thus the SOL current should technically be determined from self consistent simulations rather than from post-processing. Although for the current work the SOL current is post-processed, this timescale result gives reason to be cautious in the interpretation of SOL currents, and is extra motivation to use the right self consistent boundary condition in JOREK in the future.

Besides being relevant for how the SOL current can be simulated, the self induction timescale also has control implications. As long as the SOL current is $I_{SOL} > 1$kA, then signals with frequency $f = 10$Hz can be measured by the divertor shunt (see section 2.3). In that case the self induction is the limiting factor of the diagnostic frequency, and it constitutes it's own block in the control loop between "Detachment state" and "Divertor cassette dynamics". It means that changes in the detachment state can only be discerned on timescales of SOL self induction.

### 4.1.3 Implementation of SOL current post-processing tool in JOREK

To determine the SOL current in ITER, first a number of (R,Z) starting points per toroidal angle $\phi$ and per finite element along the boundary are chosen (in this work, 1 angle and 1 position per element, so 482 starting positions). For each of these starting points, a fieldline tracer takes small steps in phi in the direction of the magnetic field $\mathbf{B}$, keeping track of the integrals $\sigma_{\parallel,av}$, $L$, and the pressure term integral in equation 4.1. Once the connecting side is reached, the starting and ending temperatures are compared to determine $T_h$, $T_c$, $n_h$ and $n_c$ and to correct the sign of the integrals if the starting point was the cold side of the fieldline.

Then all terms in equation 4.1 are known except $\hat{j}_\parallel$, which appears on both sides of the equation. To find $\hat{j}_\parallel$, a custom Newton solver was implemented where the error function is equation 4.1 with the right hand side moved to the left, which adjusts both the stepsize and the initial guess in order not to violate the limits on $\hat{j}_\parallel$ due to the logarithmic term. The derivative of the error function was determined analytically, and the stepsize was limited to avoid oscillating guesses without convergence. In this way, $\hat{j}_\parallel$ is always found in a reasonable timespan.

From $\hat{j}_\parallel$, the current density into the wall $j_{wall}$ is calculated after which this current density is integrated over the area on the wall represented by one point. The target current is then the sum over these currents per point, where only those points are selected which are on the target using an array mask based on the points' (R,Z) coordinates. This is done for both targets, resulting in two estimates of the SOL current which should be equal.

The SOL routine takes about 2 minutes per time step, i.e. tracing and solving equation 4.1 for the 482 starting positions. This means that a single run can generally be post-processed with ms time resolution within a few hours. The limiting factor in the performance is that the pressure gradient integral needs very fine resolution as the fluctuations in $1/n\mathrm{d}p_e/\mathrm{d}s_\parallel$ happen over length scales far smaller than the element sizes, thus to resolve the integral well, the toroidal step size of the fieldline tracer must be small.

### 4.1.4 Benchmark of JOREK's SOL current post-processing tool

To check that the SOL current post-processing tool works correctly, it was confirmed that $L \approx 2\pi Rq = O(100\mathrm{m})$, with $q$ the safety factor, and $\sigma_{\parallel,av} \approx \sigma_{\parallel,Spitzer}$ were of the right order of magnitude, that the integral over the pressure gradient $\int \mathrm{d}p_e/\mathrm{d}s_\parallel \mathrm{d}s_\parallel = \Delta p_e$ equals the difference in pressure between

the two targets, and that fieldline integrals for tracers starting at the inner target gave the same result as for those starting at the outer target (see figure 4.1), which is essentially a convergence check. As mentioned previously, this requires small toroidal steps for the line tracer, especially for $j_\parallel$, due to the fluctuations in the $p_e$ term in equation 4.1. Furthermore, it was checked that $\hat{j}_\parallel$ stayed within its physical limits; for positive $j_\parallel$, ion current is drawn to the cold side, so the saturation limit imposes $j_\parallel < en_c c_{sc}$, meaning $\hat{j}_\parallel < (n_c c_{sc})/(n_h c_{sh})$, which was never violated. The resulting total current to the inner target was $I_{SOL,IT} = 23.8$kA and from the outer target $I_{SOL,OT} = 23.7$kA, thus $I_{SOL}$ was of the expected order of magnitude [14], and the error $\sigma(I_{SOL}) \approx 0.1$kA which is less than 1% and thus negligible.

The target current density (figure 4.1) was also compared to earlier results from SOLPS (see figure 4.2), where a scan of impurity seeding rates with argon produced a range of results for different SOL states. Although there is no seeding in the JOREK runs done in this work, the SOLPS results give an idea of the expected target current density profiles. It can be seen that JOREK's SOL current routine $j_{wall}$ is of the same order of magnitude $\sim 1\text{kA/m}^2$, the shapes are similar with both having a small opposite sign peak near the separatrix and a long tail into the far SOL of order 0.5m, and the differences between the two targets in sign, amplitude and extent into the far SOL are also similar. These similarities between this result with the JOREK routine and the previous result from SOLPS give confidence that the SOL current routine is working correctly.

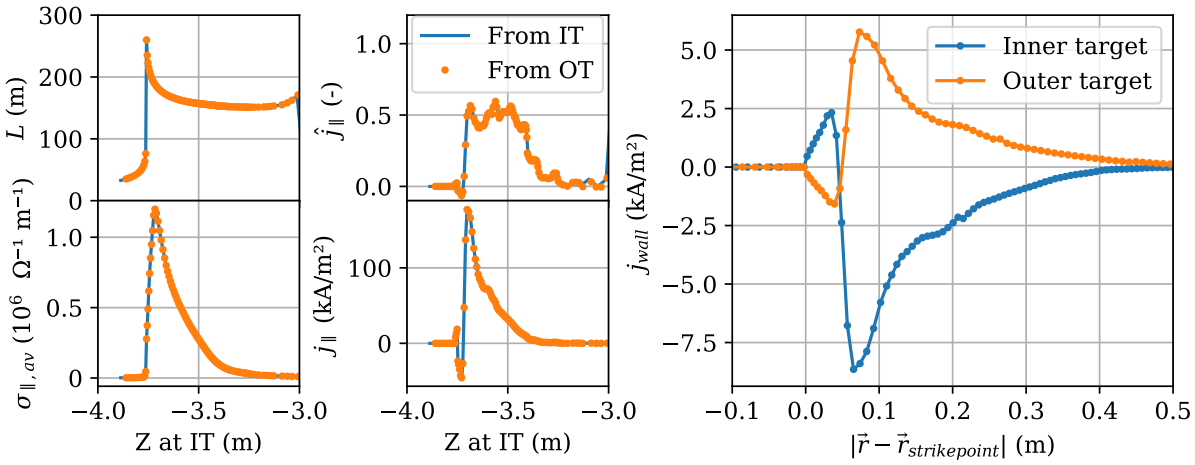


*Figure 4.1: Results from the SOL current routine for last time step of transient run (see figure 3.8, orange dotted profiles). Left: intermediate results, showing that quantities calculated for a fieldline are the same for tracers starting at the inner target and ending at the outer target as for tracers starting at the outer target. Furthermore $L$, $\sigma_{\parallel,av}$ and $\hat{j}_\parallel$ are of the expected order of magnitude. Right: calculated target current density (positive means current flows out of the target into the SOL), which compares well to the range of results found in previous work (figure 4.2). The total current was $I_{SOL} = 23.8$kA with 0.1kA difference between inner and outer target, which is negligible. Thus the SOL routine passed all sanity checks and its results can be considered reasonable.*

## 4.2 Preparation for acquiring transfer function

In this section the preparations to extract a lightweight data-driven model from JOREK simulations are discussed. First the basic idea of using system identification to extract a transfer function will be discussed, followed by the used implementation of dynamic puffing.

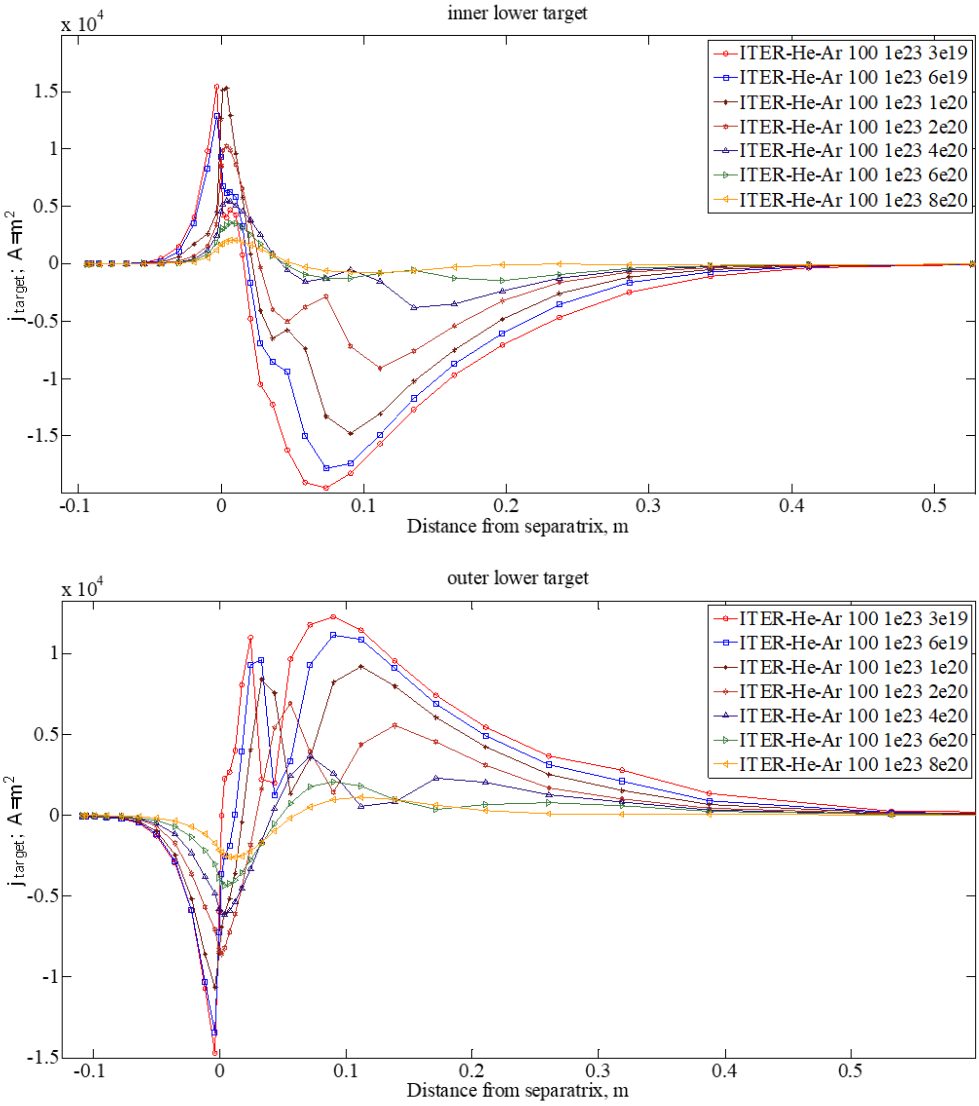


*Figure 4.2: SOL current densities on the targets for SOLPS runs with increasing argon seeding and thus increasingly detached SOL state for inner (top figure) and outer (bottom figure) targets. It can be seen that the current density on the target calculated with JOREK's SOL current routine (figure 4.1) falls in the range of results observed for SOLPS. Profile shape, magnitude, and difference between inner and outer target all correspond to results for SOLPS, thus validating the results of the JOREK SOL current routine as reasonable. Figures kindly prepared by EG Kaveeva.*

### 4.2.1 Theory on acquiring a transfer function

A transfer function is a way to describe a linear time-invariant system by describing the output, in our case SOL current $I_{SOL}(t)$, as a function of sinusoidal input of different frequencies, in our case the puff rate $\Phi(t)$ in the Laplace domain, where both the amplification of the input signal $|H(s)|$ and the phase shift between input and output signal $\angle H(s)$ are captured as a function of the complex frequency $s$.

$$H(s) = \mathcal{L}(\Phi(t))/(\mathcal{L}(I_{SOL}(t)) = \Phi(s)/I_{SOL}(s) \tag{4.17}$$

Although the SOL system is globally non-linear, for instance due to the different non-linear states the SOL can be in such as attached or detached, if the SOL system behaves linear locally, then the

system near an equilibrium can still be described adequately with a transfer function. Local linearity means that for small changes $\delta\Phi(t)$ around an equilibrium puff rate $\Phi_{eq}$, the output of a sum of input signals must be the sum of the outputs of the different components of the input signal

$$H(s)(\delta\Phi_1(s) + \delta\Phi_2(s)) \stackrel{!}{=} H(s)\delta\Phi_1(s) + H(s)\delta\Phi_2(s) \tag{4.18}$$

E.g. a step up should give opposite response to a step down, and scaling the magnitude of a step should lead to equal scaling in the response.

A priori it is not clear whether the SOL system is indeed locally linear around a semi-detached equilibrium, so this must be investigated. Since it is known that the physics model is currently lacking fidelity, this is left for future work. If it turns out that the system is locally linear, then the corresponding transfer function can be determined by perturbing the equilibrium puff rate with sinusoidal puff rates of different frequencies and seeing the response, thus generating a frequency response function (FRF). A FRF essentially contains the magnitude and phase shift of the output signal with respect to the input signal, so that it represents discrete points of the transfer function. With enough points, the transfer function can thus be determined. This process is for example shown in [35].

To determine the frequency response, it is necessary to be able to puff dynamically, which is discussed in the next subsection.

### 4.2.2 Implementation and testing of dynamic puffing in JOREK for this work

Previous to this work, there was a coding module in which full dynamic puffing was implemented, but this only become known to the authors of this work after results had already been gathered. Thus this work used a custom built dynamic puff rate implementation, which for completion is reported here.

To keep the puff rate fully flexible in this duplicate implementation, it was chosen to implement the dynamic puff rate capability by reading $(t, \Phi)$ points from a file and linearly interpolating between consecutive points for simulation times intermediate to specified rates to get a piecewise linear $\Phi(t)$. The file can either be written by hand for simple signals with only a few points, or it can be written from code in for instance python. If necessary, different puff locations can use different puff rate files. Once the simulation starts, the puff rate files are loaded with some basic sanity checks like $\Phi > 0$ atoms/s and t solely increases. During the simulation, the index of the largest $t_{puff} \leq t_{sim}$ is stored, so that the search for the current time step is shortened.

To test whether the dynamic puff rate implementation works correctly, the realised puff rates as printed in the output file are plotted together with the specified puff rate in the input file in figure 4.3, where indeed it can be seen that the linear interpolation works as planned. Note that arbitrarily many points can be used in the puff rate input file, so that for the rest of the simulations in this work, sinusoidal puff rates are approximated very well.

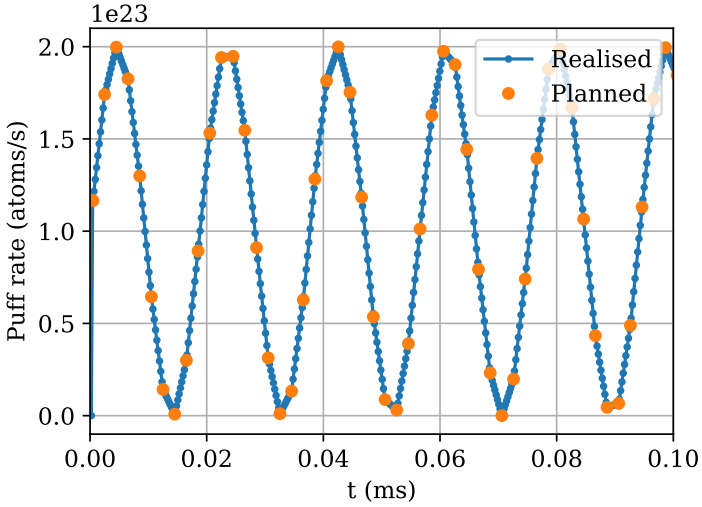


*Figure 4.3: Test of the dynamic puff rate implementation. The realised puff rate (blue) at each simulation time step (blue markers) is the linear interpolation of the requested puff rate (orange), as was indeed the goal.*

# Chapter 5:

# Proof of concept preliminary control results for ITER using JOREK

In this chapter the dynamic response of the SOL will be investigated as a proof that JOREK can be used to investigate these things, and to gain an initial low fidelity insight into control quantities. First the GNSS with $\mathbf{E} \times \mathbf{B}$ drift will be discussed, followed by simulations with a step up in the puff rate and a sinusoidal puff rate.

## 5.1 Obtaining global near steady state with drift

The run from which the GNSS with $\mathbf{E} \times \mathbf{B}$ drift was obtained is similar to the run from which the GNSS without drifts was obtained (see section 3.4.3). Contrary to that run, now an absorption coefficient of 99% performed best, compared to the 50% necessary without drifts. This is likely caused by the $\mathbf{E} \times \mathbf{B}$ drift moving particles to the outboard side, meaning the concentration is lowered in the PFR where the pump is located.

The time evolution of this run is shown in figure 5.1, where it can be seen that after 40ms, profiles start to saturate, so that later the simulation can be considered GNSS. At the end, the SOL is still mostly attached as can be seen from the high temperature, low density and nearly unchanged sheath heat flux. This is undesired as the control relevant regime is the semi-detached SOL. However, given the current state of the JOREK code with the ad hoc tuning of the pumping coefficient, and the lack of much larger SOLPS upstream densities, the method used to reach this GNSS cannot be used effectively to gain a semi-detached GNSS. Therefore the best method to gain a semi-detached GNSS is to first improve JOREK, with neutral-neutral collisions as a priority so that the pumping coefficient does not have to be tuned ad hoc anymore. This is left for future work, while in this work the current GNSS is used for proof of concept preliminary results.

It can also be seen that the simulation with drift has larger imbalance between the inner and outer targets than the simulations without drifts. This is expected from the role of the $\mathbf{E} \times \mathbf{B}$ drift which pushes energy to the outboard side thus making it easier for the inboard side to enter the high recycling and detached regime than the outboard target.

The sheath heat flux on the target ($q_{sheath} = 8kT_e n_e |\mathbf{v}_{\parallel} \cdot \mathbf{n}|$) is the plasma contribution to the heat flux on the target which is caused by the sheath potential. It does not contain wall recombination, neutral or radiation contributions, which means that it only represents the total target heat flux well for attached or semi-detached plasmas, not for highly detached plasmas. This is also true for later mentions of $q_{sh}$ in this chapter. Since most $q_{peak}$ are still quite large, likely the only place where the approximation is off is for the low values seen in figure 5.2.

To speed up the process of reaching GNSS, the puffed neutrals were initiated on the separatrix of both divertor legs. As changing the puff location would change the SOL and thus require equilibration, the two dynamic responses discussed in this chapter keep the puff location at the separatrix, as they start from this GNSS. This means that the response is somewhat faster in these simulations than when neutrals are puffed from the top, but this difference is only of the order 5ms.

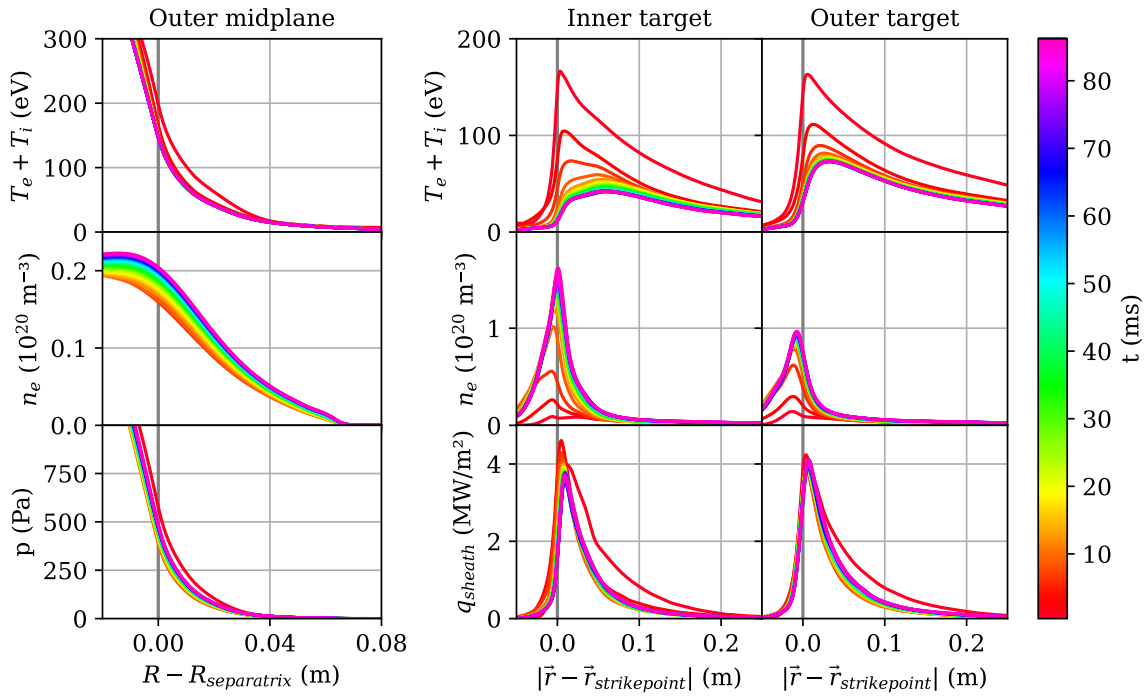


*Figure 5.1: Global near steady state run time evolution with drifts. In contrast to the without drifts case (see section 3.4.3) which required 50% absorption coefficient, this GNSS with* $\mathbf{E} \times \mathbf{B}$ *drift required 99% for GNSS. This increase is necessary as the drift moves the particles outward, leaving lower concentrations in the PFR where the pump is located. At the targets, the profiles saturate after* $\sim 40$ms*, meaning that at the end the simulation can be considered to be in GNSS. From the high target temperatures, low target density and high target heat fluxes, it can be seen that the SOL is still attached at the end, which is not the regime of interest for control. The difference between inner and outer target density and temperature is larger for the reached GNSS with drift than without drifts (figure 3.8 dark green lines) as is expected from the role of the* $\mathbf{E} \times \mathbf{B}$ *drift which moves more energy to the outer target thus keeping it more strongly attached while the inner target already starts recycling more.*

## 5.2 Insights from a step up in the gas puff rate

Since the GNSS was mostly attached, the step up response is relevant as it detaches the SOL whereas a step down response is not. At $t = 86$ms, i.e. the end of the GNSS generation, the puff rate was multiplied by 4. The resulting $I_{SOL}(t)$ as calculated with the SOL current routine describe in chapter 4, and the peak sheath heat flux are shown in figure 5.2.

Initially, $I_{SOL}$ creeps up, meaning there is some non linear behaviour of $I_{SOL}$ for an attached plasma, which might well be caused by the transition from low to higher recycling. Then $I_{SOL}$ drops down to near 0 with a decay time of about 30ms. At the inner target, the peak sheath heat flux drops down nearly instantly while the outer target takes far longer to respond. This is comparable to observations of current day devices [36] and SOLPS simulations [19], in which the inner target detaches sooner than the outer target, as explained in section 2.1.1.

For the outer target, the dominating decay timescale of $\sim 50$ms is likely the timescale with which the upstream density is pushed up. This depends on the particle content of the simulation, thus on the integral of the puff rate. This could be tested by seeing how the decay time at the outer target corresponds with the amplitude of the puff rate step, as a larger puff rate step means a faster growing integral.

The responses of both $I_{SOL}$ and $q_{sh,peak}$ do not show unstable behaviour in the form of an expo-

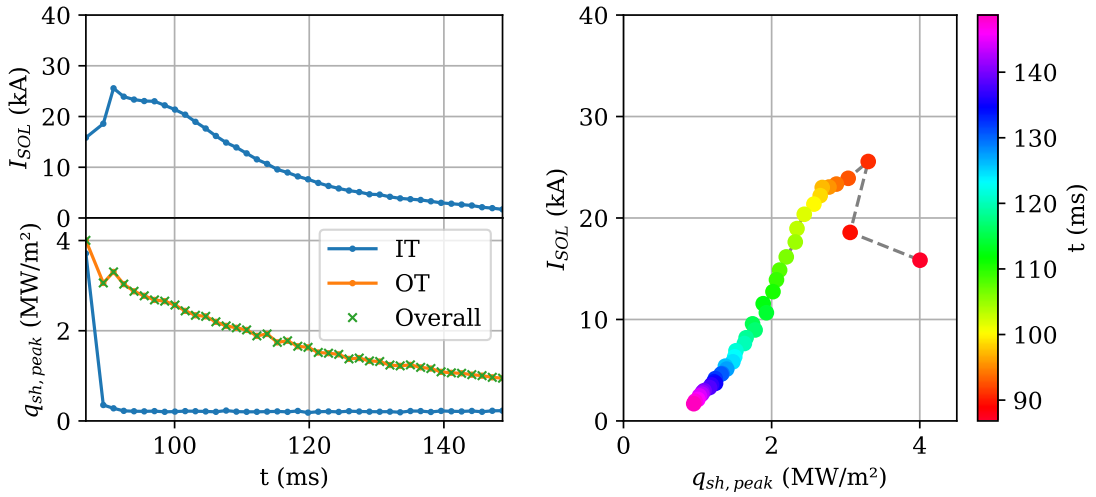


*Figure 5.2: Results from a step up in the puff rate from $\Phi_{eq} = 70 \cdot 10^{21}$atoms/s (see figure 5.1) to $\Phi = 280 \cdot 10^{21}$atoms/s. After initial non-linear behaviour, the SOL current and the peak sheath heat flux both drop, meaning that if the behaviour were linear and response times equal, it would be possible to determine $q_{sh,peak}(t)$ from $I_{SOL}(t)$. Furthermore, it can be seen that the inner target responds very fast, while the outer target takes longer to respond, likely on the timescale of increase in upstream density which depends on the number of injected particles. These results are to be taken lightly due to the model's lack of fidelity.*

nential runaway process. Since a step response in principle excites all frequencies, this should mean the SOL system is not linearly unstable.

The resulting relation between the post-processed $I_{SOL}(t)$ and $q_{sh,peak}(t)$ is one-to-one, once the initial attached regime is left. Further investigation would be required to check that the relation stays the same for other dynamic puff rates such as different step sizes and sinusoidal rates.

## 5.3 Insights from a sinusoidal gas puff rate

As the GNSS with $\mathbf{E} \times \mathbf{B}$ drift is still mostly attached, the average amplitude of the sinusoidal gas puff was larger ($\Phi_{av} = 140 \cdot 10^{21}$atoms/s) than the GNSS puff rate ($\Phi_{eq} = 70 \cdot 10^{21}$atoms/s). This causes the SOL to slowly detach over time, meaning that at the beginning of the simulation, the response is more like the response of an attached plasma, and later it is more like the response of a semi-detached plasma. The sinusoidal had a period of 40ms, and started at $t = 0$, but since the GNSS ended at $t = 86$ms, the phase at the start of the dynamic response is not 0, meaning that the gas puff is suddenly increased significantly by the non-zero value of the sinusoid. In the future it would be better to start the dynamic response simulation at 0 phase.

Results are shown in figure 5.3 for the time domain and relation between $q_{sh,peak}$ and post-processed $I_{SOL}$. In figure 5.4, the frequency response is shown, with the discrete (fast) Fourier transform amplitude and phase difference (compared to the puff rate phase), for both $q_{sh,peak}$ and $T_{e,peak}$. Note that the puff rate has period $T = 40$ms, thus the frequency $f = 25$Hz is the excited frequency.

From the results it can be seen that the response of the SOL to changes in the puff rate is fast, namely of order 5ms. This is visible from the near instant change in $q_{sh,peak}$ at the beginning, and from the small difference between the peaks of the puff rate compared to the lows of $I_{SOL}$ and $q_{sh,peak}$ and vice versa. The fact that the response is fast can also be seen from the phase difference in the frequency response at $f = 25$Hz. Perfect anti-correlation, i.e. phase $\pm\pi$ would mean an instant reaction as increasing the puff rate should decrease both $q$ and $T_e$, so the fact that the amplitude peaks at $f = 25$Hz are the largest peaks (after $f = 0$Hz, which is the equilibrium response), and their

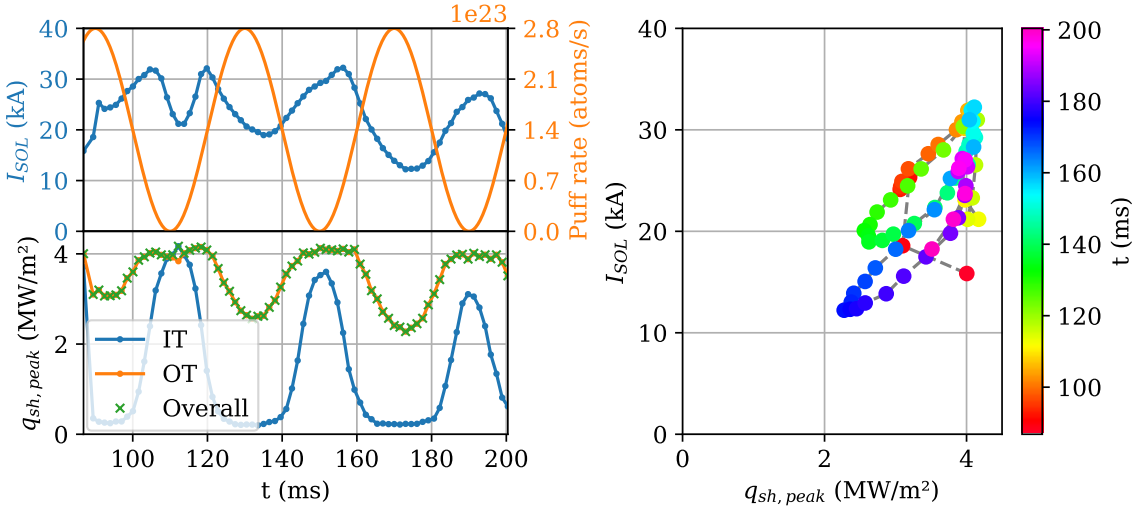


*Figure 5.3: Results from a sinusoidal puff rate starting from GNSS with drift. The response time, e.g. characterised by the difference between peaks and $I_{SOL}(t)$ and lows in $q_{sh,peak}(t)$, is less than* 5ms*, which is small compared to diagnostic and actuator timescales. The peaks in OT and lows in IT $q_{sh,peak}$ behave nonlinear as that target is then attached or detached respectively. Also $I_{SOL}(t)$ behaves nonlinearly at the start of the run. The resulting $I_{SOL}$ vs $q_{sh,peak}$ graph shows correlation but no one-to-one relation. These results are to be taken lightly due to the model's lack of fidelity.*

phase is very close to $-\pi$ shows that the timescale is short too. In figure 5.3, $q_{sh,peak}$ seems slightly faster in its response to the puff rate than post-processed $I_{SOL}$ but this difference of ∼2ms is negligible, especially compared to the here not included SOL self induction timescale of ∼0.1s.

As mentioned, the nonzero phase and the step up in average puff rate causes nonlinear behaviour at the beginning of the simulation. This is most clearly visible for $I_{SOL}$, which initially rises, similar to the initial rise in $I_{SOL}$ seen in figure 5.2, followed by a local dip at $t = 110$ms. Besides these initial nonlinear effects, also in $q_{sh,peak}$, there is nonlinear behaviour at the OT for lows in the puff rate (when the OT is strongly attached) and at the IT for highs in the puff rate (when the IT is detached). This actually gives rise to a moment in which the IT $q_{sh,peak}$ is larger than on the OT at $t \sim 110$ms, which is likely caused by the IT having larger $\mathbf{b} \cdot \mathbf{n}$ and smaller area, thus larger peak heat flux for strongly attached cases. These nonlinearities due to the large amplitude can also be seen as local peaks at $f = 50$Hz (twice the excited frequency) in the frequency domain (figure 5.4), as that signals a periodic but nonlinear response. This all is reason to use smaller puff rate amplitudes in future identification experiments.

Another observation is that the transient induced by the doubling of average puff rate can be seen, for instance in figure 5.3 by the lowering of the lows in OT and highs in IT $q_{sh,peak}$, and the transient lowering of the $I_{SOL}$ sinusoid from $t > 140$ms onward. The transient can also be clearly seen in the frequency response, where there are significant peaks even outside multiples of the excited frequency, especially at low frequency. This decay with frequency is typical for transients. In principle the transient could be filtered out, for instance using a local polynomial method [37], however, the resolution of the data is not great as the simulation spanned less than two periods. This could easily be improved in the future by letting the simulation run for longer.

Since there are these nonlinearities in the output signal, these results cannot be used as a datapoint in a transfer function as explained in section 4.2.1. Nevertheless, the nonlinearities are explainable by SOL state regimes and the transient, thus the system may well be locally linear. This would require further investigation to confirm. Once confirmed, future system identification experiments should start from a semi-detached initial GNSS, and the amplitude of the puff rate perturbation should be small

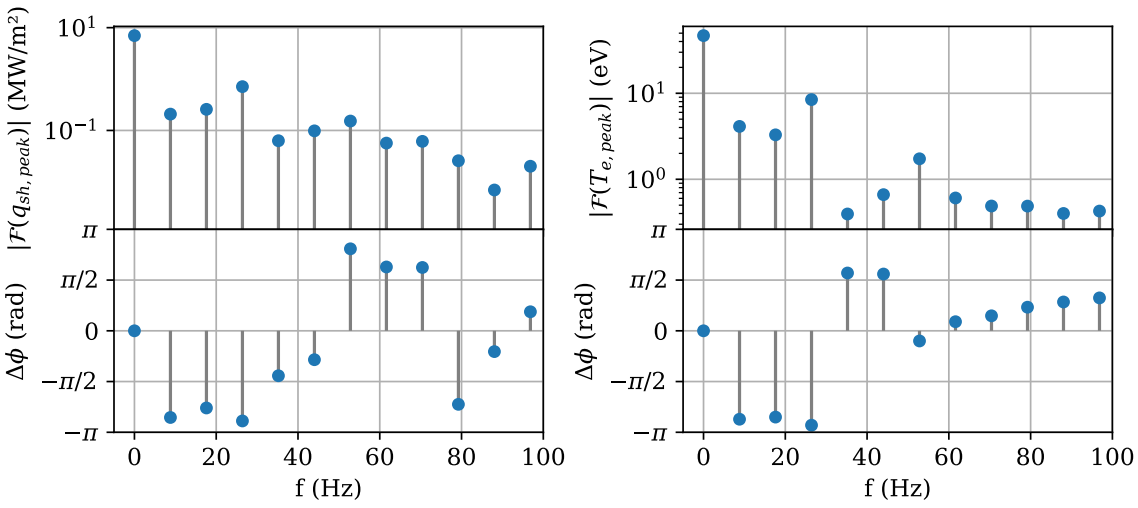


*Figure 5.4: Frequency response of the overall peak sheath heat flux (left) and outer target peak electron temperature (right) to the sinusoidal puffing rate with $T = 40$ms, meaning $f = 25$Hz. Both amplitude (up) and phase difference between that quantity and the puff rate (down) are shown. Although the $25$Hz response is the largest peak after the constant $f = 0$Hz response, both the amplitudes and the phase differences show that there is noise from the transient and nonlinearities.*

in order to stay in the locally linear regime.

Another interesting result is the lack of unstable behaviour, such as an exponentially growing mode. To the contrary, in figure 5.3, $I_{SOL}$ and both target's $q_{sh,peak}$ are bounded, with the transient slowly lowering their response over time as expected. This adds to the conclusion in the previous section that the system is likely not linearly unstable to changes in the puff rate.

Lastly, after the initial nonlinear phase passed, $q_{sh,peak}(t)$ and $I_{SOL}(t)$ show strong correlation, i.e. lower $q_{sh,peak}$ generally means lower $I_{SOL}$. This correlation is visible despite the large amplitude of the gas puff and the transient in the SOL state. Although the relation between $q_{sh,peak}$ and $I_{SOL}$ is not one-to-one, given the drawbacks it is reasonably close to one-to-one, thus these results are promising and motivate further investigation.

# Chapter 6:
# Discussion and conclusion

In this work kinetic neutral JOREK was used to study detachment dynamics for ITER. First, results of the kinetic neutral model were compared to the established equilibrium code SOLPS, which showed problems in JOREK's results. After improving the kinetic neutral model's heat transport, particle conservation and adding a pump, JOREK's model still produced different results to SOLPS, likely due to the missing neutral-neutral collisions and molecules in JOREK's model.

Further improvements to JOREK were considered out of scope for this project. Instead the focus was shifted to produce the setup to investigate detachment control dynamics, so that this setup could be used once JOREK's model was improved further. This included building a SOL current post-process routine. In doing so, it was found that the SOL current has a significant self induction timescale of $\sim$0.1s. With this setup, proof of concept results were determined, which showed short $\sim$5ms SOL system timescales and correlation between $q_{peak}(t)$ and post-processed $I_{SOL}(t)$, albeit not one-to-one.

## 6.1 Initial implications of preliminary results

The observed SOL system timescale $\sim$5ms is much smaller than the actuator timescale $\sim$500ms and the diagnostic timescale which is dominated by the SOL self induction timescale $\sim$0.1s. This agrees with findings from present day devices and previous research into SOL timescales in ITER, where SOL timescales of order ms are often quoted [38, 39, 40].

This small SOL timescale has two consequences. First, given that the system timescale is not slower than the actuator + diagnostic timescales, the ability for the given control loop to keep the SOL state within operational boundaries stays an open question. This depends on 1) whether the SOL state is stable on the timescale of the actuator and 2) whether disturbances on the SOL state caused by the interaction with the core are slow and/or gentle enough to be controlled by the control loop.

For subquestion 1), this work hints that the SOL state is likely stable, although this would require further investigation to establish as fact.

For subquestion 2, these disturbances can for example be a change in power entering the SOL, L-H transition (low confinement mode to high confinement mode), or a change in upstream (impurity) density for instance due to pellet fuelling of the core, etc. For all such disturbances, either the timescale of the process should be longer than the time scale of the closed control loop, as then it can be controlled, or the effect should be small enough that it is possible to keep the SOL state within operational limits despite fast perturbations to the SOL state. Investigating this in detail would require dynamic numerical codes in which the core and the SOL are well coupled. Therefore kinetic neutral JOREK, which inherently models the full (core + SOL) plasma self consistently, is well suited to investigate such issues once the model's fidelity is increased.

Second, the kind of instant step up in the puff rate or sinusoidal puff rate with period $T = 40$ms in the vessel is not realistically possible with a 20m long puff pipe as these fast fluctuations will average out while the gas puff travels from the valve to the vessel. Therefore it can be expected that the SOL state will have near instant response compared to the puff rate period. As such, the SOL system response (i.e. its transfer function) can be approximated as time independent, and thus it can effectively be modelled as a static (nonlinear) gain for control purposes. This is beneficial as lightweight models are easier and faster to work with from a control perspective.

On the diagnostic side, there was correlation between post-processed $I_{SOL}(t)$ and $q_{sh,peak}(t)$. However, due to the long self-induction timescale of the SOL current compared to the system timescale, the true (non post-processed) response of $I_{SOL}(T)$ has much more delay than $q_{sh,peak}$. Thus there

is bound to be hysteresis in a fast changing dynamic $q_{peak}$ vs $I_{SOL}$, as $q_{peak}$ will change and saturate before $I_{SOL}$, i.e. the curve $(q_{peak}, I_{SOL})(t)$ will move horizontally before it moves vertically, so a single $I_{SOL}$ could mean a whole range of corresponding $q_{peak}$, making it difficult to use divertor shunt measurements of $I_{SOL}(t)$ as a diagnostic of $q_{peak}(t)$. Thus the divertor shunt can only be used as diagnostic if there are no fast changes in the SOL plasma. Since the actuator is slower than the diagnostic, this diagnostic delay can be considered a correction on the response time of the closed loop, which is mainly governed by the actuator.

For all measured $I_{SOL}$ the divertor cassette sensitivity limit at low ($\sim$1Hz) frequency of 0.1kA is easily satisfied by more than an order of magnitude, meaning that $\sim$10Hz frequencies, requiring $I_{SOL} \geq$ 1kA, could be measured from the point of view of the divertor cassette as well. Since the observable frequency is faster than the self induction timescale, the limiting factor of the divertor shunt diagnostic is the self induction timescale rather than the divertor cassette dynamics.

Note that the stability issues discussed here are different from a loss of puffing (order SOL system timescale, i.e. $\sim$5ms) or loss of seeding event ($\sim$0.1s [7]), which have to be caused by a mechanical failure of a puff valve rather than by normal operation. There are already control systems designed which keep the puff rates stable even if a valve fails, by detecting the failure through a lack of pressure in the respective pipe, and compensating that with other pipelines. The conclusion from the short timescales involved in those processes is that if that control system somehow fails, this will be detected by the divertor shunt after it is already too late to act upon.

## 6.2 Further research

During this project, the following possible areas of further research were identified:

1. Improving the physics in JOREK's kinetic neutral model. As discussed at length in section 3.6, there are a lot of possibilities to push JOREK's kinetic neutral model forward, with the goal of acquiring a trustworthy high fidelity time dependent SOL simulation code, which can be used to study all kinds of problems for ITER and other devices relating to the problem of heat exhaust. Besides the obvious applications of improving estimates of the system timescales and of the $q_{peak}$ vs $I_{SOL}$ relation mentioned before, this could for instance also be used to see whether future devices such as ITER could run using an XPR (X point radiator) as solution to the exhaust problem, and how to maneuver the SOL into either an XPR or a semi-detached state after start-up.
2. Besides improving JOREK's kinetic neutral model, it should also be rigorously benchmarked against experiment, and not just in equilibrium but also the time evolution should be verified. To do this would require well diagnosed gas cut shots in an existing tokamak. Such shots have been proposed to AUG recently, exactly for the purpose of benchmarking dynamic SOL codes.
3. This work was not yet successful in acquiring a transfer function of the ITER SOL system, although it showed initial results that the transfer function can likely be approximated by a non-linear static gain. Determining the transfer function well would require both model improvement, implementing the SOL current boundary condition correctly, and acquiring a semi-detached equilibrium. Then, the linearity of the local equilibrium, which is interesting for the control engineer by itself, should be confirmed, after which small amplitude ($\sim 10 \cdot 10^{21}$atoms/s) slow sinusoidal ($T >$ 0.1s) perturbations with multiple frequencies could be used for determining the transfer function.
4. As discussed in the previous section, the short SOL system timescale $\sim$5ms naturally leads to the follow up research question whether the resulting system can still be controlled well enough to keep the SOL state within operational boundaries. This would require investigation into the timescale and effect of all possible disturbances on the SOL state, to see whether the SOL state is stable enough on the timescale of the control loop >0.5s.

## 6.3 Wider relevance of this work

In the introduction, the question posed was *What are the basics of SOL dynamics relevant to ITER detachment control with divertor shunts as diagnostic?* As JOREK's model still misses important physics, there are only preliminary answers to this question, namely: (I) there is correlation between $q_{peak}$ and $I_{SOL}$, but details require further investigation. (II) The timescale of the SOL system is ∼5ms. (III) No transfer function is determined yet, but due to the small timescale, system transfer functions can be approximated by a static nonlinear gain, the mapping of which requires further investigation. (IV) Since the SOL timescale is much faster than the actuator and diagnostic timescales, being able to keep the SOL state within operational boundaries requires the perturbations on the SOL state to be slow and/or gentle enough. This requires further investigation. In addition, there have been no findings contradicting the possibility to control the SOL with the given feedback loop, as there were for example no observed instabilities during the simulation.

The research question can thus not be answered conclusively, both because the proof of concept results are not final results, and because the proof of concept results do not fully answer the research question.

Nevertheless, this work proved the concept that these kind of questions can be studied with JOREK's model, thus being a motivation to improve JOREK and study such questions further in the future. That is all relevant to ITER and similar future devices.

Besides showing a proof of concept answer to the research sub questions, this work contributed to the dynamic SOL modelling capability by improving on JOREK's kinetic neutral model (chapter 3). This is not just relevant for ITER detachment control, but is useful for any dynamic high fidelity simulation of a fusion SOL plasma, in any magnetic confinement device, even for example for JOREK stellarator simulations when boundary physics is important. In fact some of these improvements have already been taken up within the JOREK community to simulate dynamic detachment and XPR's in Asdex Upgrade (AUG). Furthermore the SOL current routine is relevant for low frequency (larger than self-induction timescale) SOL current estimations with JOREK for any device in which such currents are of interest.

Therefore, this work contributed both to detachment controller design in ITER, which is required to operate ITER, and to dynamic magnetic confinement fusion SOL simulations in general, thus this work helped bring the reality of nuclear fusion power a step closer to this world in desperate need of reliably available sustainable energy.

## 6.4 Conclusion

This work improved the promising JOREK's kinetic neutral model, and produced proof of concept control results for ITER. Correlation was found between $q_{peak}$ and $I_{SOL}$, albeit not a one-to-one relation. Furthermore a fast SOL system response timescale of ∼5ms compared to the actuator timescale of ∼0.5s and the divertor shunt response time, which is dominated by the SOL self induction timescale with upper estimate of ∼0.1s.

This means the SOL system can likely be modelled well by a non-linear gain for control purposes, and more research into the perturbations on the SOL system are required for definitive conclusions on the controllability of the SOL system using the divertor shunt as diagnostic and gas puff as actuator.

In the future, when JOREK's kinetic neutral model is improved, this work can be built upon to gain higher fidelity control results.

# Acknowledgement

I would like to express gratitude towards all who helped this project in any way. I received great supervision from Timo Ravensbergen and Javier Artola on a daily basis at ITER and while writing my report. They were not just professionally good supervisors, but they also made me feel welcome and at home at ITER. Also thanks to Roger Jaspers for all the supervision from the side of the TU/e. Besides insights from official supervisors, I had many useful discussions with Andrei Pshenov (ITER), Sven Korving (TU/e) and Richard Pitts (line manager ITER), so I thank you for your time and attention. Thank you also Sven Korving and Chris Orrico for letting me use code you produced and helping me understand it. Thanks also to DIFFER, who allowed me to use code for determining the FRF, even though in the end the data was not suitable for it. I am also grateful to the JOREK team for useful discussions, support and interest, and generally for being a great community, including Guido Huijsmans who even came to ITER for a live discussion. Thanks to everyone at ITER who helped my internship be a great time. I would also like to thank Liza Kaveeva, who kindly prepared a figure for this report. Naturally, I also want to thank Sasja, my wife, who did not only put her studies on hold to leave for France with me, but also supported me at every step including when nothing seemed to work and all simulations crashed. And finally, I want to thank God, in whom we live and have our being, who was there at every step, and who created the universe, encouraging us to investigate it in awe and wonder.

# Bibliography


[1] A. S. Kukushkin, H. D. Pacher, R. A. Pitts, Characteristics of divertor detachment for ITER conditions, Journal of Nuclear Materials 463 (2015) 586–590. doi:10.1016/j.jnucmat.2014.10.042.

[2] R. Rossi, M. Gelfusa, T. Craciunescu, L. Spolladore, I. Wyss, E. Peluso, J. Vega, C. F. Maggi, J. Mailloux, M. Maslov, A. Murari, Jet Contributors, A systematic investigation of radiation collapse for disruption avoidance and prevention on JET tokamak, Matter and Radiation at Extremes 8 (4). doi:10.1063/5.0143193.

[3] M. Lehnen, K. Aleynikova, P. B. Aleynikov, D. J. Campbell, P. Drewelow, N. W. Eidietis, Y. Gasparyan, R. S. Granetz, Y. Gribov, N. Hartmann, E. M. Hollmann, V. A. Izzo, S. Jachmich, S. H. Kim, M. Kočan, H. R. Koslowski, D. Kovalenko, U. Kruezi, A. Loarte, S. Maruyama, G. F. Matthews, P. B. Parks, G. Pautasso, R. A. Pitts, C. Reux, V. Riccardo, R. Roccella, J. A. Snipes, A. J. Thornton, P. C. De Vries, Disruptions in ITER and strategies for their control and mitigation, Journal of Nuclear Materials 463 (2015) 39–48. doi:10.1016/j.jnucmat.2014.10.075.

[4] S. Q. Korving, G. T. Huijsmans, J. S. Park, A. Loarte, Development of the neutral model in the nonlinear MHD code JOREK: Application to e × B drifts in ITER PFPO-1 plasmas, Physics of Plasmas 30 (4). doi:10.1063/5.0135318.

[5] ITER Organization, ITER Research Plan within the Staged Approach (Level III-Provisional Version), Tech. rep. (2018).

[6] D. Humphreys, G. Ambrosino, P. De Vries, F. Felici, S. H. Kim, G. Jackson, A. Kallenbach, E. Kolemen, J. Lister, D. Moreau, A. Pironti, G. Raupp, O. Sauter, E. Schuster, J. Snipes, W. Treutterer, M. Walker, A. Welander, A. Winter, L. Zabeo, Novel aspects of plasma control in ITER, Physics of Plasmas 22 (2). doi:10.1063/1.4907901.

[7] X. Bonnin, R. A. Pitts, V. Komarov, F. Escourbiac, M. Merola, L. Bo, L. Wei, L. Pan, A. S. Kukushkin, ITER divertor plasma response to time-dependent impurity injection, Nuclear Materials and Energy 12 (2017) 1100–1105. doi:10.1016/j.nme.2017.03.010.

[8] I. H. Hutchinson, Principles of Plasma Diagnostics, 2nd Edition, Cambridge University Press, 2002.

[9] O. Schmitz, Spectroscopic measurements in the plasma edge and scrape off layer, Fusion Science and Technology 61 (2 T) (2012) 402–410. doi:10.13182/FST12-A13527.

[10] M. Bernert, Analysis of the H-mode density limit in the ASDEX Upgrade tokamak using bolometry.

[11] H. Meister, M. Bernert, W. Biel, M. Han, L. C. Ingesson, K. Mukai, F. Penzel, B. J. Peterson, R. Reichle, M. L. Reinke, S. Schmitt, D. Zhang, Bolometer developments in diagnostics for magnetic confinement fusion, Journal of Instrumentation 14 (10). doi:10.1088/1748-0221/14/10/C10004.

[12] O. Février, C. Theiler, H. De Oliveira, B. Labit, N. Fedorczak, A. Baillod, Analysis of wall-embedded Langmuir probe signals in different conditions on the Tokamak à Configuration Variable, Review of Scientific Instruments 89 (5). doi:10.1063/1.5022459.
URL `http://dx.doi.org/10.1063/1.5022459`

[13] A. Kallenbach, A. Carlson, G. Pautasso, A. Peeters, U. Seidel, H. P. Zehrfeld, Electric currents in the scrape-off layer in ASDEX Upgrade, Journal of Nuclear Materials 290-293 (2001) 639–643. doi:10.1016/S0022-3115(00)00445-1.

[14] C. A. Orrico, T. Ravensbergen, R. A. Pitts, X. Bonnin, E. Kaveeva, J. S. Park, V. Rozhansky, I. Senichenkov, C. Watts, M. De Baar, Evaluation of ITER divertor shunts as a synthetic diagnostic for detachment control, Nuclear Fusion 63 (8). doi:10.1088/1741-4326/acd947.

[15] R. A. Pitts, X. Bonnin, F. Escourbiac, H. Frerichs, J. P. Gunn, T. Hirai, A. S. Kukushkin, E. Kaveeva, M. A. Miller, D. Moulton, V. Rozhansky, I. Senichenkov, E. Sytova, O. Schmitz, P. C. Stangeby, G. De Temmerman, I. Veselova, S. Wiesen, Physics basis for the first ITER tungsten divertor (8 2019). doi:10.1016/j.nme.2019.100696.

[16] X. Bonnin, W. Dekeyser, R. Pitts, D. Coster, S. Voskoboynikov, S. Wiesen, Presentation of the New SOLPS-ITER Code Package for Tokamak Plasma Edge Modelling, Plasma and Fusion Research 11 (2016) 1–6. doi:10.1585/pfr.11.1403102.

[17] P. C. Stangeby, The Plasma Boundary of Magnetic Fusion Devices, Taylor & Francis, 2000.

[18] T. Eich, A. W. Leonard, R. A. Pitts, W. Fundamenski, R. J. Goldston, T. K. Gray, A. Herrmann, A. Kirk, A. Kallenbach, O. Kardaun, A. S. Kukushkin, B. Labombard, R. Maingi, M. A. Makowski, A. Scarabosio, B. Sieglin, J. Terry, A. Thornton, Scaling of the tokamak near the scrape-off layer H-mode power width and implications for ITER, Nuclear Fusion 53 (9). doi:10.1088/0029-5515/53/9/093031.

[19] A. A. Pshenov, A. S. Kukushkin, S. I. Krasheninnikov, On detachment asymmetry and stability, Physics of Plasmas 24 (7). doi:10.1063/1.4991402.
URL http://dx.doi.org/10.1063/1.4991402

[20] A. Loarte, B. Lipschultz, A. S. Kukushkin, G. F. Matthews, P. C. Stangeby, N. Asakura, G. F. Counsell, G. Federici, A. Kallenbach, K. Krieger, A. Mahdavi, V. Philipps, D. Reiter, J. Roth, J. Strachan, D. Whyte, R. Doerner, T. Eich, W. Fundamenski, A. Herrmann, M. Fenstermacher, P. Ghendrih, M. Groth, A. Kirschner, S. Konoshima, B. Labombard, P. Lang, A. W. Leonard, P. Monier-Garbet, R. Neu, H. Pacher, B. Pegourie, R. A. Pitts, S. Takamura, J. Terry, E. Tsitrone, Chapter 4: Power and particle control, Nuclear Fusion 47 (6). doi:10.1088/0029-5515/47/6/S04.

[21] A. Kallenbach, M. Bernert, R. Dux, L. Casali, T. Eich, L. Giannone, A. Herrmann, R. McDermott, A. Mlynek, H. W. Müller, F. Reimold, J. Schweinzer, M. Sertoli, G. Tardini, W. Treutterer, E. Viezzer, R. Wenninger, M. Wischmeier, Impurity seeding for tokamak power exhaust: From present devices via ITER to DEMO, Plasma Physics and Controlled Fusion 55 (12). doi:10.1088/0741-3335/55/12/124041.

[22] D. Brida, D. Silvagni, T. Eich, M. Faitsch, P. McCarthy, Role of electric currents for the SOL and divertor target heat fluxes in ASDEX Upgrade, Plasma Physics and Controlled Fusion 62 (10). doi:10.1088/1361-6587/aba8d6.

[23] J. A. Snipes, R. Albanese, G. Ambrosino, R. Ambrosino, V. Amoskov, T. C. Blanken, S. Bremond, M. Cinque, G. De Tommasi, P. C. De Vries, N. Eidietis, F. Felici, R. Felton, J. Ferron, A. Formisano, Y. Gribov, M. Hosokawa, A. Hyatt, D. Humphreys, G. Jackson, A. Kavin, R. Khayrutdinov, D. Kim, S. H. Kim, S. Konovalov, E. Lamzin, M. Lehnen, V. Lukash, P. Lomas, M. Mattei, A. Mineev, P. Moreau, G. Neu, R. Nouailletas, G. Pautasso, A. Pironti, C. Rapson, G. Raupp, T. Ravensbergen, F. Rimini, M. Schneider, J. M. Travere, W. Treutterer, F. Villone, M. Walker, A. Welander, A. Winter, L. Zabeo, Overview of the preliminary design of the ITER plasma control system, Nuclear Fusion 57 (12). doi:10.1088/1741-4326/aa8177.

[24] R. J. Pearce, A. Antipenkov, B. Boussier, S. Bryan, M. Dremel, B. Levesy, C. Mayaux, M. Wykes, The ITER divertor pumping system, design evolution, simplification and performance, Fusion Engineering and Design 88 (6-8) (2013) 809–813. doi:10.1016/j.fusengdes.2013.01.050.

[25] M. Hoelzl, G. T. Huijsmans, S. J. Pamela, M. Bécoulet, E. Nardon, F. J. Artola, B. Nkonga, C. V. Atanasiu, V. Bandaru, A. Bhole, D. Bonfiglio, A. Cathey, O. Czarny, A. Dvornova, T. Fehér, A. Fil, E. Franck, S. Futatani, M. Gruca, H. Guillard, J. W. Haverkort, I. Holod, D. Hu, S. K. Kim, S. Q. Korving, L. Kos, I. Krebs, L. Kripner, G. Latu, F. Liu, P. Merkel, D. Meshcheriakov, V. Mitterauer, S. Mochalskyy, J. A. Morales, R. Nies, N. Nikulsin, F. Orain, J. Pratt, R. Ramasamy, P. Ramet, C. Reux, K. S rkim ki, N. Schwarz, P. Singh Verma, S. F. Smith, C. Sommariva, E. Strumberger, D. C. Van Vugt, M. Verbeek, E. Westerhof, F. Wieschollek, J. Zielinski, The JOREK non-linear extended MHD code and applications to large-scale instabilities and their control in magnetically confined fusion plasmas, Nuclear Fusion 61 (6). doi:10.1088/1741-4326/abf99f.

[26] S. Wiesen, D. Reiter, V. Kotov, M. Baelmans, W. Dekeyser, A. S. Kukushkin, S. W. Lisgo, R. A. Pitts, V. Rozhansky, G. Saibene, I. Veselova, S. Voskoboynikov, The new SOLPS-ITER code package, Journal of Nuclear Materials 463 (2015) 480–484. doi:10.1016/j.jnucmat.2014.10.012.

[27] J. S. Park, X. Bonnin, R. Pitts, Assessment of ITER divertor performance during early operation phases, Nuclear Fusion 61 (1) (2021) 16021. doi:10.1088/1741-4326/abc1ce.
URL https://doi.org/10.1088/1741-4326/abc1ce

[28] A. S. Kukushkin, A. R. Polevoi, H. D. Pacher, G. W. Pacher, R. A. Pitts, Physics requirements on fuel throughput in ITER, Journal of Nuclear Materials 415 (1, Supplement) (2011) S497–S500. doi:https://doi.org/10.1016/j.jnucmat.2010.08.050.
URL https://www.sciencedirect.com/science/article/pii/S0022311510004411

[29] A. S. Kukushkin, H. D. Pacher, V. Kotov, D. Reiter, D. P. Coster, G. W. Pacher, Effect of the dome on divertor performance in ITER, Journal of Nuclear Materials 363-365 (1-3) (2007) 308–313. doi:10.1016/j.jnucmat.2007.01.094.

[30] A. V. Chankin, S. Clement, L. De Kock, S. K. Erents, J. Harbour, J. A. Tagle, journalof nuclear materials Parallel currents in the scrape-off layer of JET diverted discharges, Journal of Nuclear Materials (1992) 739–744.

[31] F. L. Hinton, Collisional Transport, in: M. N. Rosenbluth, R. Z. Sagdeev (Eds.), Colissional tranport in plasmas, 1st Edition, North-Holland Publishing Company, 1983, Ch. 1.5. doi:10.1201/9780429502804-8.

[32] A. S. Richardson, NRL Plasma Formulary (2019).

[33] R. Dengler, Self inductance of a wire loop as a curve integral, Advanced Electromagnetics 5 (1) (2016) 1–8. doi:10.7716/aem.v5i1.331.

[34] F. J. Artola, K. Lackner, G. T. Huijsmans, M. Hoelzl, E. Nardon, A. Loarte, Understanding the reduction of the edge safety factor during hot VDEs and fast edge cooling events, Physics of Plasmas 27 (3). doi:10.1063/1.5140230.

[35] T. Ravensbergen, M. van Berkel, A. Perek, C. Galperti, B. P. Duval, O. Février, R. J. van Kampen, F. Felici, J. T. Lammers, C. Theiler, J. Schoukens, B. Linehan, M. Komm, S. Henderson, D. Brida, M. R. de Baar, Real-time feedback control of the impurity emission front in tokamak divertor plasmas, Nature Communications 12 (1). doi:10.1038/s41467-021-21268-3.

[36] S. Potzel, M. Wischmeier, M. Bernert, R. Dux, H. W. Müller, A. Scarabosio, A new experimental classification of divertor detachment in ASDEX Upgrade, Nuclear Fusion 54 (1). doi:10.1088/0029-5515/54/1/013001.

[37] M. Van Berkel, R. J. Van Kampen, G. Vandersteen, T. Kobayashi, T. Ravensbergen, H. Igami, J. T. Lammers, G. W. Oosterwegel, C. Galperti, F. Felici, M. R. De Baar, LHD Experiment Group, TCV Team, Correcting for non-periodic behaviour in perturbative experiments: Application to heat pulse propagation and modulated gas-puff experiments, Plasma Physics and Controlled Fusion 62 (9). doi:10.1088/1361-6587/ab9eaa.

[38] A. S. Kukushkin, H. D. Pacher, G. W. Pacher, V. Kotov, R. A. Pitts, D. Reiter, Impact of potential narrow SOL heat flux on H-mode access in ITER, Nuclear Fusion 53 (12). doi:10.1088/0029-5515/53/12/123024.

[39] E. Kaveeva, V. Rozhansky, I. Senichenkov, I. Veselova, S. Voskoboynikov, X. Bonnin, D. Coster, Speed-up of SOLPS-ITER code for tokamak edge modeling, 45th EPS Conference on Plasma Physics, EPS 2018 2018-July (2018) 1452–1455.

[40] G. W. Pacher, H. D. Pacher, G. Janeschitz, A. S. Kukushkin, ITER operation window determined from mutually consistent core-SOL-divertor simulations: Definition and application, Nuclear Fusion 48 (10). doi:10.1088/0029-5515/48/10/105003.